

Cell-density independent increased lymphocyte production and loss rates post-autologous HSCT

Mariona Baliu-Piqué^{1*}, Vera van Hoven^{2*}, Julia Drylewicz^{1*}, Lotte E. van der Wagen³, Anke Janssen¹, Sigrid A. Otto¹, Menno C. van Zelm⁴, Rob J. de Boer⁵, Jürgen Kuball^{1,3}, José A.M. Borghans^{1*} and Kiki Tesselaar^{1*}

¹Center for Translational Immunology, University Medical Center Utrecht, The Netherlands;

²Department of Experimental Immunology, Amsterdam UMC, University of Amsterdam, The Netherlands;

³Department of Hematology, University Medical Center Utrecht, The Netherlands;

⁴Department of Immunology and Pathology, Monash University and Alfred Hospital, Melbourne;

⁵Theoretical Biology, Utrecht University, Utrecht, The Netherlands

*These authors contributed equally to this work

Corresponding author:

Kiki Tesselaar, PhD

Center for Translational Immunology

University Medical Center Utrecht (UMCU)

P.O. Box 85090, 3508 AB Utrecht, The Netherlands

T: +31 (0)88755394; E-mail: K.Tesselaar@umcutrecht.nl

Abstract

Lymphocyte numbers need to be quite tightly regulated. It is generally assumed that lymphocyte production and lifespan increase homeostatically when lymphocyte numbers are low, and vice versa return to normal once cell numbers have normalized. This widely-accepted concept is largely based on experiments in mice, but is hardly investigated in vivo in humans. Here we quantified lymphocyte production and loss rates in vivo in patients 0.5-1 year after their autologous hematopoietic stem cell transplantation (autoHSCT). We indeed found that the production rates of most T-cell and B-cell subsets in autoHSCT-patients were 2 to 8-times higher than in healthy controls, but went hand in hand with a 3 to 9-fold increase in cell loss rates. Both rates also did not normalize when cell numbers did. This shows that increased lymphocyte production and loss rates occur even long after autoHSCT and can persist in the face of apparently normal cell numbers.

Introduction

Under healthy conditions, the peripheral T- and B-cell populations are maintained at relatively constant numbers throughout life^{1,2}. Homeostatic mechanisms are thought to regulate lymphocyte production and survival rates in a density-dependent manner. Indeed, studies in rodents have shown that lymphocyte division and lifespan increase in response to severe lymphopenic conditions³. Robust peripheral proliferation of T-cells occurs both upon adoptive cell transfer into severely lymphocyte-depleted mice, and in partially immune-depleted hosts in the absence of adoptive cell transfer, a phenomenon termed lymphopenia-induced proliferation (LIP)³⁻⁶. Similarly, rapid proliferation and extended survival of B-cells occur after adoptive cell transfer into B-cell deficient hosts and correlate with peripheral B-cell numbers⁷.

By analogy, it is generally assumed that lymphopenic conditions induce alterations in lymphocyte dynamics in humans. However, in humans full recovery of the T-cell compartment following an autologous hematopoietic stem cell (autoHSCT) is notoriously slow, often taking several years⁸⁻¹¹. On the basis of elevated frequencies of Ki-67⁺ cells, severe lymphopenia arising after HSCT and lymphocyte-depleting treatments has been associated with increased proliferation of naive and memory T-cells¹²⁻¹⁵. However, elevated frequencies of Ki-67⁺ cells were shown to decline within 3 to 6 months after cell depletion, despite the fact that patients were still deeply lymphopenic¹³⁻¹⁵. Furthermore, increased T-cell proliferation rates after allogeneic HSCT have been shown to correlate with the occurrence of graft-versus-host disease (GVHD) and infectious-disease-related complications¹⁴. Together, these observations question whether homeostatic mechanisms are induced to compensate for low lymphocyte numbers in humans undergoing HSCT. It remains unclear to what extent increased T-cell proliferation post-HSCT reflects a T-cell density-dependent response to lymphopenia, or an immune response triggered by therapy-related tissue damage, infectious complications, or immune activation.

To elucidate whether lymphocyte production and death rates in humans are regulated in a density-dependent manner, we used *in vivo* deuterium labelling to quantify the production and loss rates of different T- and B-cell subsets in patients who received an autologous HSCT (autoHSCT), and had no signs of clinically manifested infections or GVHD. Twelve months after autoHSCT, absolute numbers of CD4⁺ T-cells and memory and natural effector B-cells in these patients were still lower than in healthy individuals, while CD8⁺ T-cell and naive B-cell numbers had already recovered to healthy control values. Deuterium labelling revealed that the production rates of most lymphocyte subsets, even those that had already reconstituted, were significantly higher in patients post-autoHSCT than in healthy individuals. These increased rates of T- and B-cell production could only be

reconciled with the observed stable cell numbers over the study time if lymphocyte loss rates were also significantly increased. Our data therefore show that increased lymphocyte production and loss rates occur long after autoHSCT, and can even persist when a lymphocyte subset has already normalized.

Results

Heterogeneous T-cell reconstitution kinetics post-autoHSCT

To investigate whether lymphocyte production and loss depend on cell numbers during lymphopenia in humans, we quantified the production and loss rates of B- and T-cells in 6 patients who received an autoHSCT for the treatment of haematological malignancies. Patients were included in the study between 196 days and 420 days post-autoHSCT, they received deuterated water ($^2\text{H}_2\text{O}$) for six weeks, and were followed for approximately one year after start of the labelling period (Figure 1).

Patient B withdrew from the study 10 weeks after the start of $^2\text{H}_2\text{O}$ labelling due to infectious complications unrelated to participation in the study. All other patients had no complications that needed treatment during the study follow-up, which was supported by CRP levels in the normal range (Figure 2).

The sub-optimal T-cell recovery observed in the peripheral blood of patients post auto-HSCT (Figure 3A) was largely due to the slow reconstitution of CD4^+ T-cells (Figure 3B). At the start of $^2\text{H}_2\text{O}$ labelling, CD8^+ T-cell numbers had reached normal levels in most patients, whereas CD4^+ T-cell numbers remained below normal levels even 1.5 years post-autoHSCT. This resulted in an inverse $\text{CD4}:\text{CD8}$ ratio in all patients except for *patient C* (Figure 3C), who experienced extremely slow CD8^+ T-cell reconstitution (Figure 3D). Naive ($\text{CD45RO}^-\text{CD27}^+$) CD4^+ T-cell numbers remained below normal levels throughout the 2-year follow-up period, whereas memory (CD45RO^+) CD4^+ T-cells reached the lower range of normal levels around 400 days post-autoHSCT (Figure 3B). Naive and memory CD8^+ T-cell numbers were at normal or supra-normal levels at the start of the study in all patients except for *patient C* (Figure 3D). In line with cell numbers, for most patients the fractions of naive cells, central memory (CM, $\text{CD45RO}^+\text{CD27}^+$), effector memory (EM, $\text{CD45RO}^+\text{CD27}^-$) and effector ($\text{CD45RO}^-\text{CD27}^-$) T-cells differed from those in healthy controls and varied slightly over time (Figure 3E and Figure 3-figure supplement 1).

Because it is generally assumed that during lymphopenia the availability of growth and survival factors increases, which has in particular been shown for IL-7 plasma levels^{16–20}, we also determined plasma levels of IL-7 and IL-15 between 12 and 24 months post-autoHSCT. Despite the CD4^+ T-cell

lymphopenia observed in these patients, their plasma concentrations of IL-7 and IL-15 and several other cytokines were in the range of those of healthy controls (Figure 2).

Increased CD4⁺ and CD8⁺ T-cell production rates post-autoHSCT

To investigate whether low CD4⁺ T-cell numbers were associated with increased T-cell production rates, we compared the level of deuterium enrichment in the DNA of the different T-cell subsets between patients and controls. Deuterium enrichment analysis showed a relatively high level of label incorporation in patients, despite the fact that the labelling period was 3 weeks shorter for patients than for controls (Figure 4A). Using mathematical modelling (see material and methods section) we estimated the production rates of the different T-cell subsets (i.e. the number of new cells produced per day, coming from a source or peripheral cell division, divided by the number of resident cells in the population). We found that the production rates of naive and memory CD4⁺ T-cells were, respectively, 6-times and 3-times higher in patients than in controls. For naive and memory CD8⁺ T-cells, the estimated production rates were approximately 8- and 4-times higher in patients compared to controls (Figure 4B, Figure 4-source data 2), despite the fact that absolute CD8⁺ T-cell numbers had already recovered to healthy levels 12 months post-transplantation.

Increased proliferation of naive but not memory CD4⁺ and CD8⁺ T cells

T-cell production rates as measured by deuterium labelling may reflect proliferation (i.e. either occasional self-renewal or a continuous burst of cell division) of the subset of interest or an influx of cells from a source (e.g. by thymic output) or from another subset (e.g. through lymphocyte differentiation). To distinguish between these options, we first measured Ki-67 expression, a snapshot marker of recent proliferative activity which, in contrast to deuterium labelling, allows to distinguish between cell division and influx. The fraction of Ki-67⁺ cells within the naive CD4⁺ and CD8⁺ T-cell pools was significantly higher in patients compared to controls (Figure 5A). For the memory T-cell subsets, in contrast, the fraction of Ki-67⁺ cells of patients did not differ significantly from those of controls (Figure 5A). This suggests that the increased production rates of memory CD4⁺ and CD8⁺ T-cells may occur due to an increased influx from naive T-cells into the memory compartment, rather than increased T-cell division within the memory T-cell pools.

Besides increased cell division in the naive T-cell pool, increased naive T-cell production rates post-autoHSCT could in theory also be due to increased thymic output. T-cell receptor excision circles (TRECs) are commonly measured to estimate thymopoiesis. Because the average TREC content per T-cell declines with age²¹⁻²³, we measured TREC contents of naive T-cells from patients, cord blood, and young (on average 23 years of age) and aged (on average 68 years of age) healthy

individuals²⁴. The average TREC content of naive CD4⁺ T-cells in patients was approximately 10-fold higher than in aged controls, and not significantly different from that of young individuals and cord blood (Figure 5B), even though all but one of the patients were more than 50 years of age. For naive CD8⁺ T-cells, the average TREC content in patients was in the range of young and aged controls (Figure 5B). We also measured CD31 expression on naive CD4⁺ T-cells, as CD31⁺CD4⁺ T cells are known to be enriched in recent thymic emigrants (RTEs)^{25,26}. The fraction of CD31⁺ cells within the naive CD4⁺ T-cell population was slightly higher in patients than in aged controls and slightly lower than in young controls and cord blood (Figure 5C and Figure 5-figure supplement 2). For naive T-cells, the combined Ki-67, TREC and CD31 data suggest that the increased T-cell production rate post-HSCT is at least partially due to increased T-cell division. Since the increased average TREC contents and percentages of CD31⁺ cells may be a direct consequence of normal thymic output entering a smaller T-cell pool²⁷, the contribution of thymic output to the increased T-cell production rate in these patients remains unclear.

Heterogeneous B-cell reconstitution kinetics post-autoHSCT

Next, we studied the changes in B-cell dynamics following autoHSCT. Although total CD19⁺ B-cell numbers and naive (IgM⁺CD27⁻) B-cell numbers had already reached normal or even supra-normal levels by day 200 post-autoHSCT, Ig class-switched (IgM⁻CD27⁺) and IgM⁺ (IgM⁺CD27⁺) memory B-cell numbers in most patients were still below, or in the lower range of, those of healthy controls throughout the study period (Figure 6A, 6B and Figure 6-figure supplement 1).

Increased production rates of B-cells post-autoHSCT

We analysed the deuterium enrichment of the different B-cell subsets to study whether B-cell production rates were increased for subsets which were still low in cell numbers (Figure 7A). The production rates of Ig switched-memory B-cells and IgM⁺ memory B-cells were 3.5-times and 5-times higher than in controls, respectively (Figure 7B, Figure 7-source data 1 (Estimates average daily production rates B cell subsets)). Also the production rate of naive B-cells, a population that had already reconstituted to supra-normal levels, remained significantly higher than in healthy controls (Figure 7B, Figure 7-source data 1).

Because B-cell production may depend on peripheral B-cell division and on *de novo* bone marrow output, we measured Ki-67 expression and kappa-deleting recombination excision circles (KRECs), in an attempt to estimate bone marrow output. The percentages of dividing, i.e. Ki-67⁺, cells within IgM⁺ and Ig switched-memory B-cells were significantly higher in patients than in healthy individuals (Figure 7C). In contrast, the fraction of Ki-67⁺ cells within the naive B-cell subset was similar between patients and controls (Figure 7C). Although naive B-cell peripheral division rates

were not increased post-autoHSCT, their production rates were 2-times higher than in controls. The division history (measured as number of cell divisions) of the naive B-cell subsets in patients tended to be lower than in controls (although not significantly), suggesting that the output of naive B-cells from the bone marrow rather than their peripheral proliferation rate was increased after autoHSCT (Figure 7D).

Increased lymphocyte production rates are counteracted by increased lymphocyte loss rates

The increased lymphocyte production rates that we observed in patients after autoHSCT may at first sight suggest that, also in humans, lymphocyte production is regulated in a density-dependent manner. The observation that lymphocyte production rates were also elevated for subsets for which cell numbers had already normalized, however, challenges this interpretation. Another observation challenging this interpretation is that for most subsets, lymphocyte numbers increased very little over time, despite the significant increase in lymphocyte production. This suggests that lymphocyte loss rates were also significantly increased after autoHSCT.

To estimate the average loss rates of all lymphocyte subsets (i.e. the number of cells lost per day, by cell death, migration or differentiation, divided by the number of resident cells in the population), we used the average lymphocyte production rates estimated from the deuterium labelling experiments and an exponential function to describe the changes in cell numbers of each lymphocyte subset over time. For most T-cell and B-cell subsets the average loss rate was approximately 3 to 5-times higher post-autoHSCT than in healthy individuals (Figure 8, Figure-8 source data 1, Estimated average daily loss rate). For naive CD8⁺ T-cells the average loss rate was even 9.5-times higher in patients than in healthy individuals (Figure 8, Figure-8 source data 1). Thus, despite the fact that production rates are clearly increased in patients post-autoHSCT, this increased production goes hand in hand with increased lymphocyte loss rates, thereby challenging the view that it reflects a homeostatic response to low lymphocyte numbers.

Discussion

From a homeostatic viewpoint, a response to low lymphocyte numbers could take the form of increased lymphocyte production or decreased lymphocyte loss. Based on the observation that severe lymphopenia in mice is associated with increased peripheral proliferation^{3-5,18}, it is widely believed that lymphocyte production rates are increased when cell numbers are low, and normalize when cell numbers do. We have previously shown that naive T-cell production rates do not increase to compensate for the at least 10-fold decline in thymic output in elderly individuals²⁴. This could be due to the relatively small degree of naive T-cell loss observed during healthy ageing. Under more

severe conditions of lymphopenia in humans, high frequencies of proliferating lymphocytes have been observed, but these have been linked to immune activation and clinical events, e.g. GVHD and opportunistic infections ¹⁴. Thus, there is little evidence that lymphocyte numbers regulate cell production and loss rates in humans.

Our deuterium labelling study shows that in patients receiving an autoHSCT, in the absence of GVHD, clinically manifested infections and transplantation-related complications, the production rates of most T- and B-cell subsets were significantly increased 12 months after transplantation. Increased lymphocyte production rates during lymphopenia have generally been interpreted as evidence for a density-dependent response to low lymphocyte numbers ^{12,13,15,28,29}. We did two additional observations, however, that suggested that these increased lymphocyte production rates post-autoHSCT were not simply reflecting a homeostatic response to low cell numbers. Firstly, T- and B-cell production rates did not normalize when cell numbers did. Secondly, not only lymphocyte production but also lymphocyte loss rates were significantly increased post-autoHSCT. Alternatively, the observed increased lymphocyte production rates post-autoHSCT could reflect an over-representation of young lymphocytes within the lymphocyte pool, in analogy with lymphocytes in the developing immune system of children, where especially in the first year T-cells have relatively high proliferation rates ³⁰. Likewise, in mice it has been shown that newly-generated naive and memory T cells have higher production and loss rates than their established counterparts ³¹⁻³³. Finally, despite the fact that the patients in our study were included up to 12 months post-transplantation and were selected on the basis of being in good health, we cannot exclude the possibility that the increased proliferation and loss rates observed post-autoHSCT may reflect HSCT-related complications, such as the impact of initial chemo-therapy and conditioning-therapy or sub-clinical infections and inflammation, which may have gone unnoticed. In fact, the increased lymphocyte production rates may even have been a response to increased lymphocyte loss rates, which themselves may have been induced by the transplantation. Lymphocyte production would then be modulated in an effort to normalize lymphocyte numbers. Whatever the underlying explanation, the ongoing dysregulation of lymphocyte dynamics in itself is an important observation. It shows that normalized cell numbers cannot be taken as an indication that homeostasis has been restored.

The observation that lymphocyte loss rates were increased post-autoHSCT is quite remarkable in the light of the widely held view that homeostatic mechanisms could take the form of increased lymphocyte survival. This concept is supported by the observation that the availability of pro-survival and anti-apoptotic factors, such as IL-7 ³⁴⁻³⁶, typically increases during lymphopenia. In our cohort, we found no evidence for increased IL-7 plasma levels, consistent with the observation that lymphocyte loss rates in these patients were not decreased. It remains unclear why IL-7 plasma levels were not increased in our cohort. A possible explanation could be that IL-7 production was hampered

by transplantation-related damage to, for example stromal cells or intestinal epithelial cells, which are an important source of IL-7³⁵⁻³⁷. We found that lymphocyte loss rates were up to 10-fold increased after autoHSCT. Although in the current study we did not take into account markers of cell death, the estimated increased cell loss rates are in line with previous human studies on T-cell survival after allogenic HSCT, which consistently reported that the fraction of pro-apoptotic cells increases following transplantation^{15,38-40}. Although this suggests that intervention with lymphocyte survival after HSCT may aid lymphocyte reconstitution, other factors apart from increased cell death may have contributed to the loss of cells from the peripheral blood. Excessive lymphocyte differentiation and/or increased migration to the tissues would also increase cell loss rates. Further studies should address whether lymphocyte reconstitution occurs at similar rates in blood and tissues in order to clarify whether lymphocyte recruitment to the tissues may be a key factor influencing the loss of lymphocytes from the blood following autoHSCT.

Consistent with previous reports^{10,15,41}, we found that 12 months post-autoHSCT, CD4⁺ T-cell numbers were below the normal range while CD8⁺ T-cells recovered more rapidly. Deuterium labelling in patients revealed that the average production rates of most T-cell subsets were significantly increased following autoHSCT. This increase was especially evident for naive T-cells. The high percentage of Ki-67⁺ naive T-cells post-autoHSCT suggests that increased naive T-cell production is to a large extent explained by increased peripheral T-cell proliferation. Memory T-cell production rates based on deuterium enrichment were also higher in patients compared to controls, while Ki-67 expression suggested that memory CD4⁺ and CD8⁺ T-cell proliferation rates were not significantly increased 0.5-1 year after autoHSCT in line with previous reports⁴². This seeming contradiction may be explained by the fact that Ki-67, a snapshot marker, may be less sensitive to detect differences in T-cell proliferation than long-term *in vivo* deuterium labelling. Alternatively, the increased production rate of memory T cells post-autoHSCT may be due to increased transition of naive T cells into the memory T-cell population. In line with this, in mice it has been demonstrated that naive T-cells adoptively transferred into immunodeficient animals can acquire a memory phenotype after antigen independent stimulation and division^{43,44}.

If a significant part of cell production in a certain lymphocyte subset (e.g. the memory subset) is indeed due to an influx from another lymphocyte subset (e.g. the naive subset), the increased production rates that we observed may either reflect a true increase in cell production, or a normal influx of cells entering a smaller lymphocyte population. To distinguish between these options, for each lymphocyte subset and each individual, we also calculated the total number of cells produced per day (i.e. coming from a source and/or from peripheral cell division), by multiplying the average production rate of each lymphocyte subset with the median cell number of that subset, and

compared these values to those in healthy controls²⁴ (Figure 3-source data 1 and Figure 4-source data 2).

We found that total daily lymphocyte production was as high as in healthy controls for naive CD4⁺ T cells and higher than in healthy controls for all other lymphocyte subsets, suggesting that the increased lymphocyte production rates post-autoHSCT truly reflected increased T-cell proliferation and/or an increased influx from another lymphocyte compartment.

Measuring thymopoiesis and the contribution of recent thymic emigrants to the naive T-cell pool after HSCT is not straightforward. Although increased TREC contents at first sight seem suggestive for increased thymic output, T-cells bearing TRECs may in fact be overrepresented in the peripheral T-cell pool post-transplantation when cell numbers are low²⁷. Hence, for naive CD4⁺ T cells, whose numbers had not yet normalized, increased average TREC contents may incorrectly be interpreted as evidence for increased thymic output. The finding that the average TREC content of naive CD4⁺ T-cells following autoHSCT was higher than in age-matched controls provides no evidence that thymic output following transplantation was higher than in healthy controls, but does imply that the thymus had become functional again within 12 months after intense conditioning for autoHSCT. The fact that the average TREC content of naive CD4⁺ T -cells, but not that of naive CD8⁺ T-cells, was higher in patients than in healthy individuals may reflect differences in the degree of depletion of naive CD4⁺ and CD8⁺ T -cells. Alternatively, it might reflect differences in the way CD4⁺ and CD8⁺ T-cells are generated. In support of the latter explanation, repertoire analyses in patients receiving an autoHSCT for the treatment of autoimmune diseases have suggested that CD4⁺ T-cells largely arise *de novo*, since most CD4⁺ T-cell clones post-autoHSCT were not present at baseline, while CD8⁺ T-cells mainly expand from cells that were already circulating pre-transplantation⁴⁵⁻⁴⁷.

To study in a population other than T-cells whether lymphocyte production and loss rates in humans are regulated in a density-dependent manner, we quantified the production and loss rates of different B-cell subsets. In line with previous reports⁴⁸⁻⁵⁰, we found that 12 months after transplantation, naive B-cell numbers had reconstituted to healthy (or even higher than healthy) control values, while Ig class-switched and IgM⁺ memory B-cells had not yet fully recovered. The delayed reconstitution of Ig class-switched and IgM⁺ memory B-cells has typically been attributed to treatment-related damage to secondary lymphoid organs, which may hamper the formation of germinal centers essential for somatic hypermutation and isotype switching⁴⁹. Also for naive, Ig class-switched, and IgM⁺ memory B-cells, we found that not only production rates but also cell loss rates were increased 12 months post-autoHSCT, further supporting our conclusion that increased lymphocyte production rates do not simply reflect a homeostatic response to low lymphocyte numbers.

In brief, our findings show that despite the slow reconstitution of lymphocytes in autoHSCT patients, lymphocyte production rates are increased. Since this increased production goes hand in hand with increased cell loss, and does not normalize when cell numbers do, it is not simply due to a homeostatic response to low cell numbers. Future studies should address whether the dynamics of lymphocytes after autoHSCT normalize in the long run, what drives the increase in lymphocyte production and loss rates during immune reconstitution, and to what extent immune reconstitution in the tissues occurs.

Materials and Methods

Key Resources Table				
Reagent type or resource	Designation	Source or reference	Identifiers	Additional information
antibody	anti-human CD45-PerCP (Mouse IgG1, κ) RRID:AB_2566358	BioLegend	Cat# 368506 Clone: 2D1	“(1:20)”
antibody	anti- human CD3-FITC (Mouse IgG1, κ) RRID:AB_2562046	BioLegend	Cat# 399430 Clone: UCHT1	“(1:25)”
antibody	anti-human CD4-APC-eF780 (Mouse IgG1, κ) RRID:AB_1272044	eBioscience	Cat# 47-0049-42 Clone: RPA-T4	“(1:50)”
antibody	anti-human CD8-V500 (Mouse IgG1, κ) RRID:AB_2870326	BD Biosciences	Cat# 561617 Clone: SK1	“(1:60)”
antibody	anti-human CD19-eFluor450 (Mouse IgG1, κ) RRID:AB_1272053	eBioscience	Cat# 48-0199-42 Clone: HIB19	“(1:25)”
antibody	anti-human CD45RO-PE-Cy7 (Mouse IgG2A, κ) RRID:AB_647426	BD Biosciences	Cat# 337168 Clone: UCHL1	“(1:60)”
antibody	anti-human CD27-APC (Mouse IgG1, κ) RRID:AB_469371	eBioscience	Cat# 17-0279-42 Clone: O343	“(1:25)”
antibody	anti-human CD31-PE (Mouse IgG1, κ) RRID:AB_400016	BD Biosciences	Cat# 340297 Clone: L133.1	“(1:12.5)”
antibody	anti-human CD3-eFluor450 (Mouse IgG2A, κ) RRID:AB_1272055	eBioscience	Cat# 48-0037-42 Clone: OKT3	“(1:50)”
antibody	anti-human CD95-PE (Mouse IgG1, κ)	BD Biosciences	Cat# 555674 Clone: DX2	“(1:50)”

	RRID:AB_396027			
antibody	anti-human CD19-PerCP (Mouse IgG1, κ) RRID:AB_2868816	BD Biosciences	Cat# 363014 Clone: SJ25C1	“(1:50)”
antibody	anti-human IgM-PE (Goat IgG) RRID:AB_2795614	Southern Biotech	Cat# 2022-09 Polyclonal	“(1:100)”
antibody	anti-human Ki-67-FITC (Mouse IgG1, κ) RRID:AB_578716	DAKO	Cat# F7268 Clone: MIB-1	“(1:10)”
Commercial assay or kit	Cytofix/Cytoperm	BD Biosciences	Cat#554714	
Commercial assay or kit	FACS Lysing Solution	BD Biosciences	Cat#349202	
Commercial assay or kit	Reliaprep Blood gDNA Miniprep System	Promega	Cat#A5081	
Commercial assay or kit	Data acquisition	Luminex	xPONENT software version 4.2	
Commercial assay or kit	Data acquisition	Biorad Laboratories	Biorad FlexMAP3D	
chemical compound	² H ₂ O, 99.8% enriched	Cambridge Isotope Laboratories	Cat#DLM-2259-1	
software, algorithm	Data analysis	Biorad laboratories	Biorad Bio-Plex Manager software, version 6.1.1	
software, algorithm	Data analysis	Biorad laboratories	Biorad FlexMAP3D	
software, algorithm	Data analysis	Westera et al. Blood 2013 DOI: 10.1182/blood-2013-03-488411	Multiexponential model	
software, algorithm	Data analysis	GraphPad PRISM	GraphPad Software	

305

306 Patient characteristics

307 Six patients who received an autoHSCT for the treatment of a hematologic malignancy were
308 enrolled in the study after having provided written informed consent. Following repeated
309 subcutaneous injections with granulocyte-colony stimulating factor (G-CSF), stem cells were obtained
310 by leukapheresis of peripheral blood. Patients received a non T-cell depleted graft; the average

number of CD34⁺ cells transplanted was 5.03x10⁶ cells/kg (median, 4.12; range, 1.82-12.38). Patients were included in the study between 196 and 420 days after autoHSCT, and had no signs of transplantation-related complications, severe infections (HIV, HBV, HCV), other liver disease, active uncontrolled infections (such as infectious mononucleosis), inadequate liver or kidney function, or cardiovascular disease before and during the study. Additional inclusion criteria were: fully transfusion-independent at start of the study, hemoglobin level ≥ 6 mmol/l, and platelet count $\geq 50 \times 10^9$ /L. Any use of medication during the study was unrelated to the malignancy and the HSCT (Figure 1). In order to compare the phenotypes of the B- and T-cell compartments of patients to those of age-matched healthy individuals, we used data from healthy individuals from a previous study²⁴, and additional blood samples were collected from healthy volunteers not following the labelling protocol after having provided informed consent. This study was approved by the medical ethical committee of the University Medical Center Utrecht and conducted in accordance with the Helsinki Declaration.

***In vivo* deuterium labelling**

In vivo deuterium labelling was performed as previously described with small adaptations²⁴. Briefly, patients received an oral ramp-up dose of 7.5 ml of heavy water (²H₂O, 99.8% enriched, Cambridge Isotope Laboratories) per kg body water on the first day of the study, and drank a daily maintenance dose of 1.25 ml ²H₂O per kg body water for 6 weeks. To reduce the study burden, the labelling period of autoHSCT patients was 3 weeks shorter than the labelling period we used in our previous study in healthy controls²⁴. Thanks to the use of the multi-exponential model, these different labelling periods for autoHSCT patients and healthy controls should not affect the estimated dynamic parameters⁵¹. Blood was withdrawn 4 times during the labelling period, and 6 times during the de-labelling period, with the last withdrawal approximately one year after the start of ²H₂O administration. Urine samples were collected during the first 13 weeks of the study and stored at -20°C until analysis. For deuterium labelling, data from healthy controls from a previous study²⁴ were used. The age of the autoHSCT patients included in the current study (median age of 54 years, see Figure 1B) was not completely matched with that of the healthy controls studied before (median age of 22 years for young, and 68 years for aged controls). Since lymphocyte dynamics hardly change with age²⁴, the comparisons in our study should not be affected by the relatively small age differences between patients and healthy controls.

Cell isolation, flow cytometry and cell sorting

Peripheral blood mononuclear cells were obtained by Ficoll-Paque (GE Healthcare, Little Chalfont, UK) density gradient centrifugation from heparinized blood. Granulocytes were obtained by

2 cycles of erythrocyte lysis (155mM NH₄Cl, 10mM KHCO₃, 0.1mM Na₂-EDTA, pH=7.0) of the granulocyte/erythrocyte layer. To determine the baseline deuterium enrichment, total peripheral blood mononuclear cells were frozen on the first day of the study, prior to ²H₂O intake.

Absolute cell numbers were determined using TruCount tubes (BD Biosciences, San Jose, CA, USA), in which whole blood was stained using CD45-PerCP (BioLegend), CD3-FITC (BioLegend), CD4-APC-eF780 (eBioscience), CD8-V500 (BD Biosciences), CD19-eFluor450 (eBioscience), CD45RO-PE-Cy7 (BD Biosciences), CD27-APC (eBioscience), and CD31-PE (BD Biosciences) antibodies. After erythrocyte lysis with FACS Lysing Solution (BD Biosciences), samples were immediately analysed.

For cell cycle analysis, we analysed the expression of the nuclear protein Ki-67. Cells were first extracellularly stained with CD3-eFluor450 (eBioscience), CD4 APC-eFluor780 (eBioscience), CD8-V500 (BD Biosciences), CD45RO-PE-Cy7 (BD), CD27-APC (eBioscience), and CD95-PE (BD Biosciences) or with CD19-PerCP (Biolegend), CD27-APC (eBioscience), and IgM-PE (Southern Biotech) monoclonal antibodies. Subsequently, cells were fixed and permeabilised (Cytofix/Cytoperm, BD Biosciences), and stained intracellularly with Ki-67-FITC (DAKO, Glostrup). Washing steps were carried out using Perm/Wash buffer (BD Biosciences). Samples were analysed on an LSR-II or LSR-Fortessa flow cytometer using FACS Diva software (BD Biosciences).

For sorting of B- and T-cell subsets, cells were incubated with CD3-eFluor450 (eBioscience), CD4 APC-eFluor780 (eBioscience), CD8-PE (Biolegend), CD19-PerCP (Biolegend), CD45RO-PE-Cy7 (BD), CD27-APC (eBioscience), and IgM-FITC (Southern Biotech). CD19⁺ naive (IgM⁺CD27⁻), Ig class-switched (IgM⁻CD27⁺) and IgM⁺ (IgM⁺CD27⁺) memory B-cells and CD3⁺CD4⁺ and CD3⁺CD8⁺ naive (CD27⁺CD45RO⁻) and memory (CD45RO⁺) T-cells were sorted on a FACS Aria II or FACS Aria III cell sorter using FACS Diva software (BD Biosciences). Flow cytometric analyses and cell sorting were always performed on freshly isolated material. Representative density dot plots and the gating strategy for TruCount and cell sorting are shown in Figure 3-figure supplement 1.

DNA isolation

Genomic DNA was isolated from sorted B- and T-cell subsets, total peripheral blood mononuclear cells and granulocytes using the Reliaprep Blood gDNA Miniprep System (Promega, Madison, WI, USA) and stored at -20°C before processing for TREC analysis or gas chromatography/mass spectrometry (GC/MS).

TREC (T-cell receptor excision circles) analysis

In sorted naive CD4⁺ and CD8⁺ T-cell samples, signal joint TREC numbers and DNA input were quantified with a ViiA™ 7 Real-Time PCR System (Applied Biosystems) as previously described²²⁴⁴. Values are the mean of two qPCR measurements of a given DNA sample.

KREC (Kappa-deleting recombination excision circle) analysis

For quantification of B-cell replication history, the KREC assay in sorted naive B-cells was performed as described previously⁴⁵. In short, genomic DNA was used as template for TaqMan-based real-time quantitative PCR of the albumin control gene, intronRSS–Kde coding joints from rearranged IGK loci, and intronRSS–Kde signal joints on KRECs. The difference in Ct values between the intronRSS–Kde coding joints and signal joints from the same sample was used to calculate B-cell replication history with technical correction Ct values obtained with the U698-DB01 control cell line⁴⁵ as follows⁴⁶:

$$(C_{T_{\text{signal joint}}} - C_{T_{\text{coding joint}}})_{\text{sample}} - (C_{T_{\text{signal joint}}} - C_{T_{\text{coding joint}}})_{\text{U698-DB01}}$$

The frequencies of cells containing an intronRSS–Kde coding joint were calculated as follows⁴⁶:

$$2^{[(C_{T_{\text{albumin}} - C_{T_{\text{coding joint}}})_{\text{sample}} - (C_{T_{\text{albumin}} - C_{T_{\text{coding joint}}})_{\text{U698-DB01}}]} \cdot 100\%$$

Multiplex immunoassay

Plasma samples were obtained from heparinized blood at different time points and stored at -80°C. Plasma levels of CRP (C-reactive protein), APRIL (A proliferation-inducing ligand or TNFSF13), FAS-L (FAS ligand or CD95L), IL-7 (Interleukin 7), IL-15 (Interleukin 15) and IL-8 (Interleukin 8 or CXCL8) were measured by a multiplex immunoassay using Luminex xMAP technology (xMAP, Luminex Austin TX USA). The assay was performed as previously described⁴⁷. Biorad FlexMAP3D (Biorad laboratories. Hercules USA) and xPONENT software version 4.2 (Luminex) were used for acquisition and data was analysed by 5-parametric curve fitting using Bio-Plex Manager software, version 6.1.1 (Biorad). Samples were measured without any previous freeze-thaw cycle. Samples of healthy controls were acquired at the same days as patient samples to take into account the effect of storage on the different plasma markers.

Measurement of deuterium enrichment in DNA and body water

Deuterium enrichment in DNA from granulocytes, sorted cells, and total peripheral blood mononuclear cells (t=0) was measured according to the method described by Busch et al.⁴⁸ with minor modifications²⁴. Briefly, DNA was enzymatically hydrolysed into deoxyribonucleotides and derivatized to penta-fluoro-triacetate (PFTA) before injection (DB-17MS column, Agilent Technologies) into the gas chromatograph (7890A GC System, Agilent Technologies). PFTA was analysed by negative chemical ionization mass spectrometry (5975C inert XL EI/CI MSD with Triple-Axis Detector, Agilent Technologies) measuring ions m/z 435 and m/z 436. For quantification of 2H enrichment, standard solutions with known enrichment (Tracer-to-Tracee ratios ([M + 1]/[M + 0]) 0, 0.0016, 0.0032, 0.0065, 0.0131, 0.0265, 0.0543, and 0.1140) were made by mixing 1-13C-deoxyadenosine (Cambridge Isotopes Inc.; generates an 'M + 1' ion) with unlabelled deoxyadenosine (Sigma, St. Louis, MO, USA). To correct for abundance sensitivity of isotope ratios, we followed the

approach proposed by Patterson et al⁴⁹ on log 10-transformed enrichment data. Deuterium enrichment in urine was analysed on the same GC/MS system (using a PoraPLOT Q 25x0.32 column, Varian) by electron impact ionization as previously described⁵⁰. Values are the mean of two GCMS measurements of a given derivative sample.

Quantification of lymphocyte dynamics by mathematical modelling of urine and DNA enrichment data and cell numbers

Mathematical models were fitted to the urine and DNA enrichment data as previously described¹⁶. The estimated maximum level of ²H enrichment in the granulocyte population of each patient was considered to be the maximum level of label incorporation that cells could possibly attain, and was used to scale the enrichment data of the other cell subsets. As cell numbers may not be constant over time during the lymphocyte reconstitution phase, we adapted the commonly used mathematical model for deuterium labeling in T and B cells by releasing the steady-state assumption. For naive T- and B-cells (N), we allow cells to be produced by the thymus for T-cells and the bone marrow for B-cells at rate σ , proliferate at a rate p_N and are lost at a rate d_N . For the other lymphocyte subsets (X), we write that they proliferate at a rate p_X and are lost at a rate d_X .

$$\frac{dN}{dt} = \sigma + p_N N - d_N N \quad (\text{eq. 1})$$

$$\frac{dX}{dt} = p_X X - d_X X \quad (\text{eq. 2})$$

The total amount of labeled DNA (L) can be modelled by the following differential equations:

$$\frac{dL_N}{dt} = \sigma cU(t) + p_N cU(t) N - d_N L_N \quad (\text{eq. 3})$$

$$\frac{dL_X}{dt} = p_X cU(t) X - d_X L_X \quad (\text{eq. 4})$$

where $U(t)$ is the fraction of deuterium in body water at time t (in days), and c is an amplification factor as previously described^{16,51}. We can derive the equations for the fraction of labeled DNA (defined by $l = L/X$) using the quotient rule of differentiation:

$$\frac{dl_N}{dt} = \left(\frac{\sigma}{N} + p_N \right) (cU(t) - l_N) \quad (\text{eq. 5})$$

$$\frac{dl_X}{dt} = p_X (cU(t) - l_X) \quad (\text{eq. 6})$$

Because of parameter identifiability issues, we were not able to estimate both σ and p_N in equation 5. We therefore made the simplifying assumption that the per cell production rate (i.e. the

number of new cells produced per day, coming from the source or peripheral cell division, divided by the number of resident cells in the population) $\left(\frac{\sigma}{N} + p_N\right)$ was not time-dependent, such that equation 6 could also be used for naive T- and B-cells. To account for potential kinetic heterogeneity in each subpopulation⁵¹, we used a multi-exponential model in which each subpopulation i contains a fraction α_i of cells with production rate p_i per day, and made the simplifying assumption that these fractions α_i are not time-dependent. The average per cell production rate p of each subpopulation was subsequently calculated as $p_X = \sum_i \alpha_i p_i$ ^{52, 53}. All subsets, except naive CD4⁺ and CD8⁺ T-cells, were significantly better described by two subpopulations. For naive CD4⁺ and CD8⁺ T-cells, only one was needed.

Equation 6 shows that deuterium enrichment data will give information only on the per cell proliferation rates p_X . To estimate the loss rates of the different lymphocyte subsets (i.e. the number of cells lost per day, by cell death, migration or differentiation, divided by the number of resident cells in the population) (d_X) we made use of cell number data. As leukocyte counts in blood are known to vary, e.g. due to diurnal rhythms, we first used a linear regression model to describe the total leukocyte numbers for each individual. To obtain cell numbers, the number of leukocytes according to this regression line was multiplied by the fraction of cells in each subset. We then fitted an exponential function to these “normalized” cell numbers for each subset and individual:

$$X(t) = X_0 e^{(p_X - d_X)t} \quad (\text{eq. 7})$$

where X_0 is the cell number at the time of inclusion in the study and p_X was fixed to the estimated values from the deuterium analyses.

Best fits of deuterium enrichment in body water and granulocytes are shown in Figure 4-figure supplement 1 and the corresponding parameter estimates are given in Figure 4-source data 1. Individual enrichment data and best fits are shown in Figure 4-figure supplement 2 for T-cells and Figure 7-figure supplement 1 for B-cells and the corresponding parameter estimates are given in Figure 4-source data 2 (T cell subsets) and Figure 7-source data 1 (B cell subsets). Normalized cell numbers and best fits are shown in Figure 8-figure supplement 1 for T-cells and Figure 8-figure supplement 2 for B-cells and the corresponding parameter estimates are given in Figure 8-source data 1.

Statistical analyses

For each individual urine and granulocyte enrichment levels were simultaneously used to estimate their respective parameters and for each lymphocyte subset deuterium enrichment data and normalized cell numbers were simultaneously used to estimate their production and loss rates.

Deuterium enrichment data were arcsin-sqrt transformed and normalized cell numbers were log10-transformed before parameter estimation. 95% confidence limits were determined by bootstrap analysis on the residuals. Parameter estimation was performed using a maximum likelihood approach using R¹⁷. Estimated medians of enrichment data, median values of longitudinal data or values of single measurements were compared between two groups using Mann–Whitney tests (GraphPad Software, Inc) or multiple groups using Kruskal-Wallis with Dunn’s correction. Differences with a p-value<0.05 were considered significant.

Acknowledgments

We thank the patients for their participation in this study, Jeroen F. van Velzen, Pien A.J. van der Burght and Gerrit Spierenburg for assistance with cell sorting, Laura Ackermans for theoretical input, Lyanne Derksen for critically reading the manuscript, Mr Benjamin Bartol and Ms Pei Mun Aui for technical support, and the nurses from the Julius Center Trial Unit for taking care of study participants.

Funding

The research leading to these results has received funding from the European Union Seventh Framework Programme (FP7/2007–2013) through the Marie-Curie Action “Quantitative T cell Immunology” Initial Training Network, with reference number FP7-PEOPLE-2012-ITN 317040-QuanTI and from the Landsteiner Foundation for Blood Transfusion Research (LSBR grant 0812).

Conflict-of-interest statements

JK has no competing interests relevant to the topic discussed. JK reports grants from Novartis, Miltenyi Biotech, and Gadeta. JK is inventor on multiple patents dealing with $\gamma\delta$ T-cell research, ligands, and isolation techniques, and is scientific co-founder and shareholder of Gadeta (Patent number: 9546998, 9891211, 10324083, 10578609. Publication number: 20200368278, 20200363397, 20190271688, 2019020961, 201901692603, 20180188234, 20170319674, 20170174741, 20150050670). All other authors declare no competing financial interests.

References

1. Lin Y, Kim J, Metter EJ, et al. Changes in blood lymphocyte numbers with age in vivo and their association with the levels of cytokines/cytokine receptors. *Immun. Ageing*. 2016;13(1):24.

- 500 2. Wertheimer AM, Bennett MS, Park B, et al. Aging and Cytomegalovirus Infection Differentially and
501 Jointly Affect Distinct Circulating T Cell Subsets in Humans. *J. Immunol.* 2014;192(5):2143–2155.
- 502 3. Freitas AA, Rocha B. Population Biology of Lymphocytes: The Flight for Survival. *Annu. Rev. Immunol.*
503 2000;18(1):83–111.
- 504 4. Miller R a, Stutman O. T cell repopulation from functionally restricted splenic progenitors: 10,000-fold
505 expansion documented by using limiting dilution analyses. *J. Immunol.* 1984;133(6):2925–32.
- 506 5. Bell EB, Sparshott SM, Drayson MT, Ford WL. The stable and permanent expansion of functional T
507 lymphocytes in athymic nude rats after a single injection of mature T cells. *J. Immunol.*
508 1987;139(5):1379–84.
- 509 6. Neujahr DC, Chen C, Huang X, et al. Accelerated Memory Cell Homeostasis during T Cell Depletion and
510 Approaches to Overcome It. *J. Immunol.* 2006;176(8):4632–4639.
- 511 7. Gaudin E, Rosado M, Agenes F, McLean A, Freitas AA. B-cell homeostasis, competition, resources, and
512 positive selection by self-antigens. *Immunol. Rev.* 2004;197:102–15.
- 513 8. Heining C, Spyridonidis A, Bernhardt E, et al. Lymphocyte reconstitution following allogeneic
514 hematopoietic stem cell transplantation: a retrospective study including 148 patients. *Bone Marrow*
515 *Transplant.* 2007;39(10):613–622.
- 516 9. Ringhoffer S, Rojewski M, Dohner H, Bunjes D, Ringhoffer M. T-cell reconstitution after allogeneic stem
517 cell transplantation: assessment by measurement of the sjTREC/ TREC ratio and thymic naive T cells.
518 *Haematologica.* 2013;98(10):1600–1608.
- 519 10. Bosch M, Khan FM, Storek J. Immune reconstitution after hematopoietic cell transplantation. *Curr.*
520 *Opin. Hematol.* 2012;19(4):324–335.
- 521 11. Williams KM, Hakim FT, Gress RE. T cell immune reconstitution following lymphodepletion. *Semin.*
522 *Immunol.* 2007;19(5):318–330.
- 523 12. Jones JL, Thompson SAJ, Loh P, et al. Human autoimmunity after lymphocyte depletion is caused by
524 homeostatic T-cell proliferation. *Proc. Natl. Acad. Sci.* 2013;110(50):20200–20205.
- 525 13. Bouvy AP, Kho MML, Klepper M, et al. Kinetics of homeostatic proliferation and thymopoiesis after ratg
526 induction therapy in kidney transplant patients. *Transplantation.* 2013;96(10):904–913.
- 527 14. Hazenberg MD. T-cell receptor excision circle and T-cell dynamics after allogeneic stem cell
528 transplantation are related to clinical events. *Blood.* 2002;99(9):3449–3453.
- 529 15. Alho AC, Kim HT, Chammas MJ, et al. Unbalanced recovery of regulatory and effector T cells after
530 allogeneic stem cell transplantation contributes to chronic GVHD. *Blood.* 2017;127(5):646–658.
- 531 16. Van Gent R, Schadenberg AWL, Otto SA, et al. Long-term restoration of the human T-cell compartment
532 after thymectomy during infancy: A role for thymic regeneration? *Blood.* 2011;118(3):627–634.
- 533 17. Sauce D, Larsen M, Fastenackels S, et al. Lymphopenia-Driven Homeostatic Regulation of Naive T Cells
534 in Elderly and Thymectomized Young Adults. *J. Immunol.* 2012;189(12):5541–5548.
- 535 18. Fry TJ, Connick E, Falloon J, et al. A potential role for interleukin-7 in T-cell homeostasis. *Blood.*
536 2001;97(10):2983–90.
- 537 19. Napolitano LA, Grant RM, Deeks SG, et al. Increased production of IL-7 accompanies HIV-1-mediated T-

cell depletion: implications for T-cell homeostasis. *Nat. Med.* 2001;7(1):73–79.

20. Bolotin E, Annett G, Parkman R, Weinberg K. Serum levels of IL-7 in bone marrow transplant recipients: relationship to clinical characteristics and lymphocyte count. *Bone Marrow Transplant.* 1999;23(8):783–788.

21. Douek DC, McFarland RD, Keiser PH, et al. Changes in thymic function with age and during the treatment of HIV infection. *Nature.* 1998;396(6712):690–695.

22. Hazenberg MD, Otto SA, Cohen Stuart JW, et al. Increased cell division but not thymic dysfunction rapidly affects the T-cell receptor excision circle content of the naive T cell population in HIV-1 infection. *Nat. Med.* 2000;6(9):1036–42.

23. Hazenberg MD, Verschuren MC, Hamann D, Miedema F, Dongen JJ. T cell receptor excision circles as markers for recent thymic emigrants: Basic aspects, technical approach, and guidelines for interpretation. *J. Mol. Med.* 2001;79(11):631–640.

24. Westera L, van Hoeven V, Drylewicz J, et al. Lymphocyte maintenance during healthy aging requires no substantial alterations in cellular turnover. *Aging Cell.* 2015;14(2):219–227.

25. Kohler S, Thiel A. Life after the thymus: CD31+ and CD31- human naive CD4+ T-cell subsets. *Blood.* 2009;113(4):769–774.

26. van den Broek T, Borghans JAM, van Wijk F. The full spectrum of human naive T cells. *Nat. Rev. Immunol.* 2018;18(June):

27. Hazenberg MD, Borghans JAM, de Boer RJ, Miedema F. Thymic output: a bad TREC record. *Nat. Immunol.* 2003;4(2):97–99.

28. Havenith SHC, Remmerswaal EBM, Bemelman FJ, et al. Rapid T cell repopulation after rabbit anti-thymocyte globulin (rATG) treatment is driven mainly by cytomegalovirus. *Clin. Exp. Immunol.* 2012;169(3):292–301.

29. Bouvy AP, Klepper M, Betjes MGH, et al. Alemtuzumab as Antirejection Therapy. *Transplant. Direct.* 2016;2(6):e83.

30. van Gent R, van Tilburg CM, Nibbelke EE, et al. Refined characterization and reference values of the pediatric T- and B-cell compartments. *Clin. Immunol.* 2009;133(1):95–107.

31. Gossel G, Hogan T, Cownden D, Seddon B, Yates AJ. Memory CD4 T cell subsets are kinetically heterogeneous and replenished from naive T cells at high levels. *Elife.* 2017;6:e23013.

32. Rane S, Hogan T, Seddon B, Yates AJ. Age is not just a number : Naive T cells increase their ability to persist in the circulation over time. 2018;1–20.

33. Reynaldi A, Smith NL, Schlub TE, et al. Fate mapping reveals the age structure of the peripheral T cell compartment. *Proc. Natl. Acad. Sci.* 2019;116(10):3974–3981.

34. Ponchel F, Cuthbert RJ, Goëb V. IL-7 and lymphopenia. *Clin. Chim. Acta.* 2011;412(1–2):7–16.

35. Barata JT, Durum SK, Seddon B. Flip the coin: IL-7 and IL-7R in health and disease. *Nat. Immunol.* 2019;20(12):1584–1593.

36. Lundström W, Fewkes NM, Mackall CL. IL-7 in human health and disease. *Semin. Immunol.* 2012;24(3):218–224.

- 576 37. Kim GY, Hong C, Park J-H. Seeing Is Believing: Illuminating the Source of In Vivo Interleukin-7. *Immune*
577 *Netw.* 2011;11(1):1.
- 578 38. Brugnani D, Airò P, Pennacchio M, et al. Immune reconstitution after bone marrow transplantation for
579 combined immunodeficiencies: down-modulation of Bcl-2 and high expression of CD95/Fas account for
580 increased susceptibility to spontaneous and activation-induced lymphocyte cell death. *Bone Marrow*
581 *Transplant.* 1999;23(5):451–457.
- 582 39. Lin MT, Tseng LH, Frangoul H, et al. Increased apoptosis of peripheral blood T cells following allogeneic
583 hematopoietic cell transplantation. *Blood.* 2000;95(12):3832–9.
- 584 40. Poulin J-F. Evidence for adequate thymic function but impaired naive T-cell survival following allogeneic
585 hematopoietic stem cell transplantation in the absence of chronic graft-versus-host disease. *Blood.*
586 2003;102(13):4600–4607.
- 587 41. Storek J, Geddes M, Khan F, et al. Reconstitution of the immune system after hematopoietic stem cell
588 transplantation in humans. *Semin. Immunopathol.* 2008;30(4):425–37.
- 589 42. Malphettes M. Evidence for naive T-cell repopulation despite thymus irradiation after autologous
590 transplantation in adults with multiple myeloma: role of ex vivo CD34+ selection and age. *Blood.*
591 2003;101(5):1891–1897.
- 592 43. Cho BK, Rao VP, Ge Q, Eisen HN, Chen J. Homeostasis-stimulated proliferation drives naive T cells to
593 differentiate directly into memory T cells. *J. Exp. Med.* 2000;192(4):549–56.
- 594 44. Goldrath AW, Bogatzki LY, Bevan MJ. Naive T cells transiently acquire a memory-like phenotype during
595 homeostasis-driven proliferation. *J. Exp. Med.* 2000;192(4):557–64.
- 596 45. Muraro PA, Douek DC, Packer A, et al. Thymic output generates a new and diverse TCR repertoire after
597 autologous stem cell transplantation in multiple sclerosis patients. *J. Exp. Med.* 2005;201(5):805–816.
- 598 46. Muraro PA, Robins H, Malhotra S, et al. T cell repertoire following autologous stem cell transplantation
599 for multiple sclerosis. *J. Clin. Invest.* 2014;124(3):1168–72.
- 600 47. Dubinsky AN, Burt RK, Martin R, Muraro PA. T-cell clones persisting in the circulation after autologous
601 hematopoietic SCT are undetectable in the peripheral CD34+ selected graft. *Bone Marrow Transplant.*
602 2010;45(2):325–331.
- 603 48. Burns LJ, Weisdorf DJ, DeFor TE, et al. IL-2-based immunotherapy after autologous transplantation for
604 lymphoma and breast cancer induces immune activation and cytokine release: A phase I/II trial. *Bone*
605 *Marrow Transplant.* 2003;32(2):177–186.
- 606 49. Avanzini MA, Locatelli F, Santos C Dos, et al. B lymphocyte reconstitution after hematopoietic stem cell
607 transplantation: functional immaturity and slow recovery of memory CD27+ B cells. *Exp. Hematol.*
608 2005;33(4):480–486.
- 609 50. Bemarck M, Holmqvist J, Abrahamsson J, Mellgren K. Translational Mini-Review Series on B cell subsets
610 in disease. Reconstitution after haematopoietic stem cell transplantation - revelation of B cell
611 developmental pathways and lineage phenotypes. *Clin. Exp. Immunol.* 2012;167(1):15–25.
- 612 51. Westera L, Drylewicz J, Den Braber I, et al. Closing the gap between T-cell life span estimates from
613 stable isotope-labeling studies in mice and humans. *Blood.* 2013;122(13):2205–2212.

52. Vrisekoop N, den Braber I, de Boer AB, et al. Sparse production but preferential incorporation of recently produced naive T cells in the human peripheral pool. *Proc. Natl. Acad. Sci.* 2008;105(16):6115–6120.
44. Hazenberg MD, Otto SA, Cohen Stuart JW, et al. Increased cell division but not thymic dysfunction rapidly affects the T-cell receptor excision circle content of the naive T cell population in HIV-1 infection. *Nat. Med.* 2000;6(9):1036-42.
45. van Zelm MC, Szczepański T, van der Burg M, van Dongen JJM. Replication history of B lymphocytes reveals homeostatic proliferation and extensive antigen-induced B cell expansion. *J. Exp. Med.* 2007;204(3):645-655.
46. van Zelm MC, van der Burg M, Langerak AW, van Dongen JJM. PID Comes Full Circle: Applications of V(D)J Recombination Excision Circles in Research, Diagnostics and Newborn Screening of Primary Immunodeficiency Disorders. *Front. Immunol.* 2011;2(MAY):1-9.
47. Scholman RC, Giovannone B, Hiddingh S, et al. Effect of anticoagulants on 162 circulating immune related proteins in healthy subjects. *Cytokine.* 2018;106(April 2017):114-124.
48. Busch R, Neese RA, Awada M, Hayes GM, Hellerstein MK. Measurement of cell proliferation by heavy water labeling. *Nat. Protoc.* 2007;2(12):3045-3057.
49. Patterson BW, Zhao G, Klein S. Improved accuracy and precision of gas chromatography/mass spectrometry measurements for metabolic tracers. *Metabolism.* 1998;47(6):706-712.
50. Westera L, Zhang Y, Tesselaar K, Borghans JAM, Macallan DC. Quantitating Lymphocyte Homeostasis In Vivo in Humans Using Stable Isotope Tracers. 2013;979:107-131.
51. Vrisekoop N, den Braber I, de Boer AB, et al. Sparse production but preferential incorporation of recently produced naive T cells in the human peripheral pool. *Proc. Natl. Acad. Sci.* 2008;105(16):6115-6120.
52. Westera L, Drylewicz J, Den Braber I, et al. Closing the gap between T-cell life span estimates from stable isotope-labeling studies in mice and humans. *Blood.* 2013;122(13):2205-2212.
53. Ganusov V V., Borghans JAM, De Boer RJ. Explicit Kinetic Heterogeneity: Mathematical Models for Interpretation of Deuterium Labeling of Heterogeneous Cell Populations. *PLoS Comput. Biol.* 2010;6(2).

Figure legends

Figure 1. Study protocol timeline and patient characteristics. (A) Summary figure depicting the study time line of every patient. Patients are centred by start of $^2\text{H}_2\text{O}$ labelling. The left bar indicated the time between the autologous hematopoietic stem cell transplantation (autoHSCT) and the start of the labelling period, the grey area indicates the 6 weeks $^2\text{H}_2\text{O}$ labelling period, the right bar provides the follow up period and the vertical bars indicate the blood sampling time points. **(B)**

Patient characteristics. Age=Age at start $^2\text{H}_2\text{O}$ labelling; M=Male; F=Female; Time post-HSCT=Reconstitution period at start $^2\text{H}_2\text{O}$ labelling; Medication usage=Medication during the study; HOVON 132 arm A (Idarubicin, Ara-C (Cytarabine), Daunorubicin); VCD (Bortezomib, Cyclophosphamide, Dexamethason); VMP (Bortezomib, Melphalan, Prednisone); VRD (Bortezomib, lenalidomide, dexamethasone); R-CHOP (Rituximab, Cyclophosphamide, Adriamycin, Vincristin, Prednisone); Ara-C (Cytarabine), TAD (Thalidomide, Adriamycin, Dexamethasone); CTD (Carfilzomib, Thalidomide, Dexamethasone); BEAM (Carmustine, Etoposide, Ara-C (Cytarabine), Melphalan). Figure 1-figure supplement 1 shows the absolute leukocytes, neutrophils, lymphocytes and monocytes numbers over time after autoHSCT.

Figure 2. Plasma levels of CRP, APRIL, FAS-L, IL-7, IL-15 and IL-8 post-autoHSCT. Plasma concentration (picogram per milliliter) of CRP (C-reactive protein), APRIL (A proliferation-inducing ligand), FAS-L (FAS ligand), IL-7 (Interleukin 7), IL-15 (Interleukin 15) and IL-8 (Interleukin 8) in patients A to F at different time points after autoHSCT. Box plots represent the distribution of values for healthy controls (n=29, box=25th-75th percentile, black line=median, whiskers=min and max values and Figure 2-source data 1: Luminex individual values plasma markers). IL-7 levels which were below the level of detection (1.3 pg/ml) were set at 1.

Figure 3. T-cell reconstitution following autoHSCT. Absolute numbers (cells per milliliter) of **(A)** total CD3⁺ T-cells, **(B)** total, naive (CD27⁺CD45RO⁻) and memory (CD45RO⁺) CD3⁺CD4⁺ T-cells, **(D)** total, naive (CD27⁺CD45RO⁻) and memory (CD45RO⁺) CD3⁺CD8⁺ T-cells and **(C)** the CD4:CD8 ratio over time for the duration of the study are depicted. Box plots represent the distribution of values for healthy controls (N=17 for CD3⁺, CD4⁺, CD8⁺ and CD4:CD8 ratio, other N=27, box=25th-75th percentile, black line=median, whiskers=min and max values). Absolute numbers shown in the graph are not normalized. **(E)** Bar graphs show the median percentage of naive (CD27⁺CD45RO⁻), central memory (CM, CD27⁺CD45RO⁺), effector memory (EM, CD27⁺CD45RO⁺) and effector (CD27⁻CD45RO⁻) CD4⁺ and CD8⁺ T-cells of autoHSCT patients (A to F) and HCs (n=6) in the indicated colors. For the T-cell subset distribution per patient over time see Figure 3-figure supplement 1 and Figure 3-source data 1. For the gating strategy see Figure 3-figure supplement 2.

Figure 4. T-cell dynamics after autoHSCT. **(A)** Deuterium enrichment in the DNA of naive and memory CD4⁺ and CD8⁺ T-cells in autoHSCT patients (A to F, color symbols), and healthy controls (HCs, grey symbols)²⁴. Dotted lines correspond to the end of the labelling period (black for autoHSCT patients and grey for HCs). Label enrichment was scaled between 0 and 100% by normalizing for the

maximum enrichment in granulocytes (See Figure 4-supplement 1 and Figure 4-source data 1: Parameter estimates urine and granulocytes). **(B)** Estimates of the per cell production rate of naive and memory CD4⁺ and CD8⁺ T-cells in autoHSCT patients and HCs ²⁴ (for individual fits and parameters estimates see Figure 4-figure supplement 2 and Figure 4-source data 2). Different symbols indicate different individuals, autoHSCT patients (A to F) in color and HCs in grey. Horizontal lines represent median values. P-values between groups are shown (Mann-Whitney test). For information on modeling in R see Figure 4-source code 1.

Figure 5. Contribution of peripheral proliferation and thymic output to T-cell production after autoHSCT. (A) Ki-67 expression was measured within naive and memory CD4⁺ (left panel) and CD8⁺ (right panel) T-cell in autoHSCT patients and HCs ²⁴(for gating strategy see Figure 5-figure supplement 1). **(B)** Average number of TRECs per naive CD4⁺ (left panel) and CD8⁺ (right panel) T-cell in autoHSCT patients, cord blood (CB) and HCs ²⁴. For *Patient A* and *Patient E*, TREC content was measured the first day of the study (t_0) as well as the last study visit (t_{end}). For *Patient D*, TREC content was not successfully measured due to limited material. **(C)** CD31 expression was measured within naive CD4⁺ T-cells in autoHSCT patients, cord blood and HCs ²⁴. For changes in CD31 expression and absolute numbers of CD31⁺ cells over time, see Figure 5-figure supplement 2. Different symbols indicate different individuals, autoHSCT patients (A to F) in color, CB in dark grey, and young (median age of 23 years) and old (median age of 68 years) HCs in light grey. Horizontal lines represent median values. P-values of differences between groups are shown (Mann-Whitney test **(A)** and Kruskal-Wallis with Dunn's correction **(B)**, comparison with CB, HC (23) and HC (68)).

Figure 6. B-cell reconstitution following autoHSCT. (A) Absolute numbers (cells per milliliter) of total CD19⁺ B-cells, naive (CD19⁺IgM⁺CD27⁻), Ig class-switched memory (CD19⁺IgM⁺CD27⁺) and IgM⁺ memory (CD19⁺IgM⁺CD27⁺) B-cells in peripheral blood over time. Graphs show the absolute cell counts per milliliter in autoHSCT patients (patients A to F) over the duration of the study. Box plots represent the distribution of values for healthy controls (N=10, box=25th-75th percentile, black line=median, whiskers=min and max values). Absolute numbers shown in the graph are not normalized. **(B)** Bar graphs show the median percentage of naive, Ig class-switched memory and IgM⁺ memory B-cells within total CD19⁺ B-cells of autoHSCT patients (patients A to F) and HCs (N=10). For the B-cell subset distribution per patient over time see Figure 6-figure supplement 1 and Figure 6-source data 1. Note the different y-axes in panel A.

Figure 7. B-cell dynamics after autoHSCT. (A) Deuterium enrichment in the DNA of B cell subsets in autoHSCT patients (A to F, color symbols), and HCs (grey symbols)²⁴. Dotted lines correspond to the end of the labelling period (black for autoHSCT patients and grey for HCs). Label enrichment was scaled between 0 and 100% by normalizing for the maximum enrichment in granulocytes (Figure 4-source data 1: Parameter estimates urine and granulocytes). **(B)** Estimates of the per cell production rates of naive, Ig class-switched memory and IgM⁺ memory B-cells in autoHSCT patients and HCs²⁴. For individual fits and estimates see Figure 7-figure supplement 1 and Figure 7-source data 1. **(C)** Ki-67 expression was measured within naive, Ig class-switched memory and IgM⁺ memory B-cells in autoHSCT patients and HCs²⁴(for gating strategy see Figure 5-figure supplement 1). **(D)** Percentage of naive B-cells containing a KREC and naive B-cell division history for autoHSCT patients and HCs²⁴. Different symbols indicate different individuals, autoHSCT patients (A to F) in color and HCs in grey. Horizontal lines represent median values. P-values of differences between groups are shown (Mann-Whitney test). For information on modeling in R see Figure 4-source code 1.

Figure 8. Average T-cell and B-cell loss rates following autoHSCT. (A) Estimates of the average loss rates of naive and memory CD4⁺ and CD8⁺ T-cells and of **(B)** naive, Ig class-switched memory and IgM⁺ memory B-cells in autoHSCT patients (A to F, color symbols), and HC (grey symbols)²⁴. Average loss rates were calculated (see Figure 8-source data 1) using the estimated average production rates and the corrected cell numbers (Figure 8-figure supplement 1 and 2) as described in material and methods. Horizontal lines represent median values. P-values of differences between groups are shown (Mann-Whitney test).

Figure supplements

Figure 1-figure supplement 1. Absolute numbers (cellsx10⁹ per liter of blood) of leukocytes, neutrophils, lymphocytes and monocytes in peripheral blood of autoHSCT patients (patients A to F) over time after autoHSCT obtained by automated blood leukocyte differential count (leukodiff). Grey areas show the range of healthy individuals' values

Figure 3-figure supplement 1. T-cell subset distribution per autoHSCT patient over time. Percentage of naive T-cells (blue), central memory T-cells (CM, orange), effector memory T-cells (EM, green) and effector T-cells (effector grey) within (A) CD4⁺ or (B) CD8⁺ T-cells at the study times after autoHSCT (patients A to F). Bar graphs for HCs (N= 6) show the median percentage of naive, CM, EM and effector T-cells within CD4⁺ or CD8⁺ T-cells.

744

745 **Figure 3-figure supplement 2. Gating strategy for TruCount and cell sorting. (A)** TruCount gating
746 strategy for naive (CD27⁺CD45RO⁻), central memory (CM, CD27⁺CD45RO⁺), effector memory (EM,
747 CD27⁺CD45RO⁺) and effector (CD27⁻CD45RO⁻) CD4⁺ and CD8⁺ T-cells and B-cells. **(B)** Gating strategy
748 for sorting for naive (CD27⁺CD45RO⁻) and memory (CD45RO⁺) CD4⁺ and CD8⁺ T-cells and for naive
749 (IgM⁺CD27⁻), Ig class-switched memory (IgM⁻CD27⁺) and IgM⁺ memory (IgM⁺CD27⁺) B-cells

750

751 **Figure 4-figure supplement 1. Best fits of ²H enrichment in (A) body water (urine) and (B)**
752 **granulocytes from the 6 autoHSCT patients (A to F). The estimated parameters for urine and**
753 **granulocytes can be found in Figure 4-source data 1.**

754

755 **Figure 4-figure supplement 2. Best fits of ²H enrichment in T-cell subsets in autoHSCT patients.** Best
756 fits of the model (see material and methods) to the enrichment data in naive and memory CD4⁺ and
757 CD8⁺ T cells in the 6 autoHSCT patients (A to F). Measured enrichments are shown by black dots.
758 Label enrichment in the DNA was scaled between 0 and 100% by normalizing for the maximum
759 enrichment in granulocytes (see material and methods). The end of ²H₂O administration is marked by
760 a dashed vertical line. Best fits of ²H enrichment of the corresponding subsets in healthy individuals
761 were previously published by Westera *et al.* 2015 ²⁴.

762

763 **Figure 4-figure supplement 3. Total daily production T-cell and B-cell subsets, calculated as (average**
764 **production rate $\left(\frac{\sigma}{N} + p_N\right) \times$ (absolute number of cells per liter of blood) \times (5 liter blood) \times 50,**
765 **assuming that 2% of lymphocytes reside in the blood ³⁴. Horizontal lines represent median values. P-**
766 **values of differences between groups are shown (Mann-Whitney test).**

767

768 **Figure 5-figure supplement 1. Gating strategy for Ki-67 expression of T and B cell subsets.** Gating
769 strategy for Ki-67 expression of naive (CD27⁺CD45RO⁻) and memory (CD45RO⁺) CD4⁺ and CD8⁺ T-cells
770 and naive (IgM⁺CD27⁻), Ig class-switched memory (IgM⁻CD27⁺) and IgM⁺ memory (IgM⁺CD27⁺) B-cells.

771

772 **Figure 5-figure supplement 2. CD31 expression in naive CD4⁺ T-cells over time.** Absolute numbers of
773 CD31⁺ naive CD4⁺ T-cells per milliliter of blood over time (left panel) and percentage CD31⁺ cells

within naive CD4⁺ T-cells (right panel). Graphs show the absolute cell counts per milliliter or the percentage CD31⁺ cells in autoHSCT patients (patients A to F, in color) over time for the duration of the study. Box plots represent the distribution of values for healthy controls (N=23, box=25th-75th percentile, black line=median, whiskers=min and max values). Absolute numbers shown in the graph are not normalized.

Figure 6-figure supplement 1. B-cell subset distribution per autoHSCT patient over time. Percentage of naive B-cells (blue), IgM⁺ memory B-cells (orange) and Ig class-switched memory B-cells (green) within total CD19⁺ B-cells per patient (patients A-F) at the study times after autoHSCT. Bar graphs for HCs show the median percentage of naive, memory and natural effector B-cells within total CD19⁺ B-cells. For the gating strategy see Figure 3-figure supplement 1

Figure 7-figure supplement 1. Best fits of ²H enrichment in B-cell subsets in autoHSCT patients. Best fits of the model (see material and methods) to the enrichment data in naive, Ig class-switched memory and IgM⁺ memory B-cells in the 6 autoHSCT patients (A to F). Measured enrichments are shown by black dots. Label enrichment in the DNA was scaled between 0 and 100% by normalizing for the maximum enrichment in granulocytes (see material and methods). The end of ²H₂O administration is marked by a dashed vertical line. Best fits of ²H enrichment of the corresponding subsets in healthy individuals were previously published by Westera *et al.* 2015²⁴.

Figure 8-figure supplement 1. Best fits of T-cell numbers in autoHSCT patients. Best fits (black lines) to the normalized cell numbers data (black dots). Absolute numbers (cells per milliliter of blood) of naive (CD27⁺CD45RO⁻) and memory (CD45RO⁺) CD4⁺ and CD8⁺ T-cells were corrected for noise as described in material and methods. The median cell numbers (dotted grey line) and the corresponding IQR (interquartile range, grey area) for healthy controls are shown.

Figure 8-figure supplement 2. Best fits of B-cell numbers in autoHSCT patients. Best fits (black lines) to the normalized cell number data (black dots). Absolute numbers (cells per milliliter of blood) of naive (CD19⁺IgM⁺CD27⁻), Ig class-switched memory (CD19⁺IgM⁻CD27⁺) and IgM⁺ memory (CD19⁺IgM⁺CD27⁺) B-cells were corrected for noise as described material and methods. The median cell numbers (dotted grey line) and the corresponding IQR (interquartile range, grey area) for healthy controls are shown.

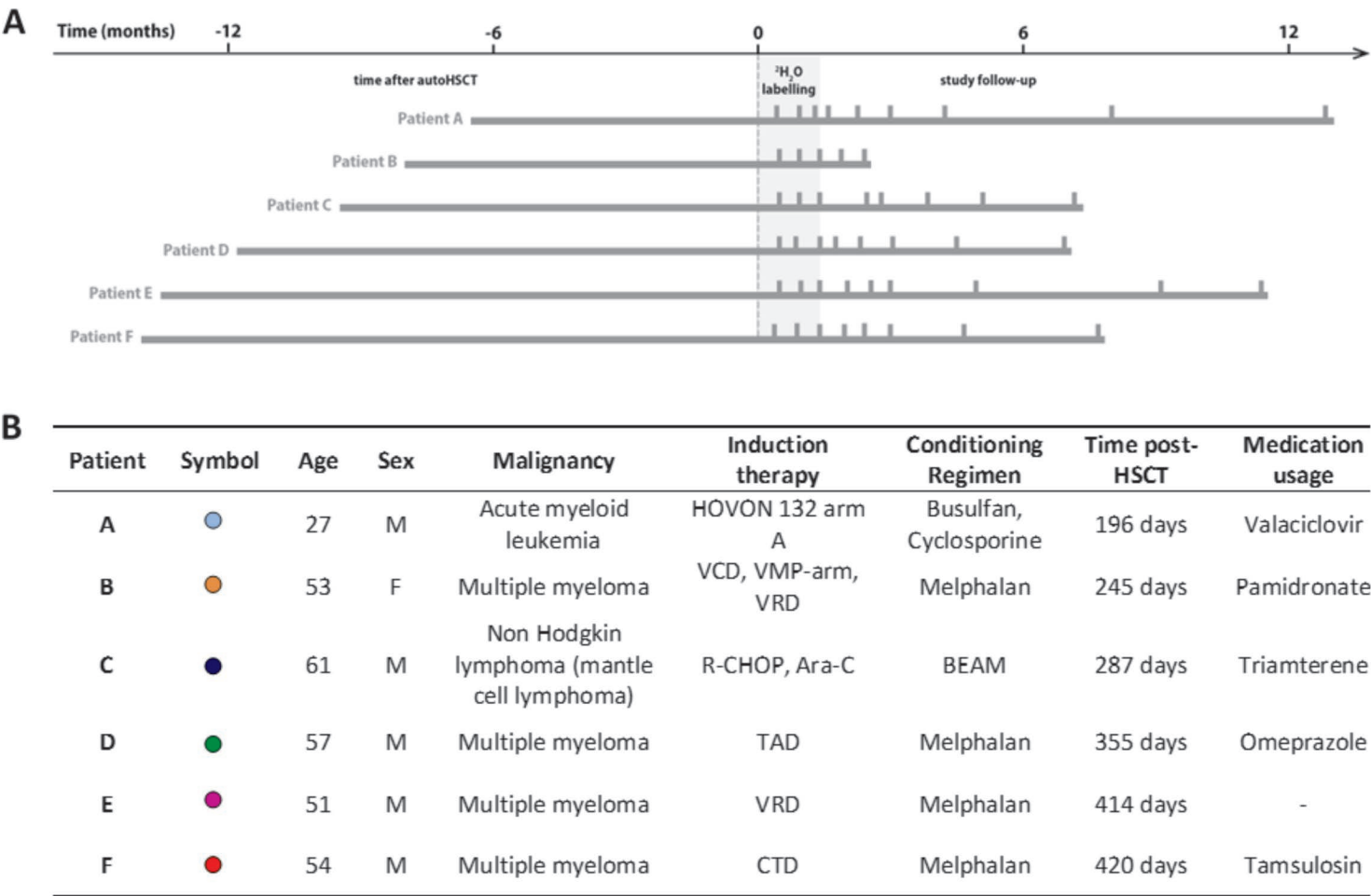


Figure 1. Study protocol timeline and patient characteristics. (A) Summary figure depicting the study time line of every patient. Patients are centred by start of $^2\text{H}_2\text{O}$ labelling. The left bar indicated the time between the autologous hematopoietic stem cell transplantation (autoHSCT) and the start of the labelling period, the grey area indicates the 6 weeks $^2\text{H}_2\text{O}$ labelling period, the right bar provides the follow up period and the vertical bars indicate the blood sampling time points. (B) Patient characteristics. Age=Age at start $^2\text{H}_2\text{O}$ labelling; M=Male; F=Female; Time post-HSCT=Reconstitution period at start $^2\text{H}_2\text{O}$ labelling; Medication usage=Medication during the study; HOVON 132 arm A (Idarubicin, Ara-C (Cytarabine), Daunorubicin); VCD (Bortezomib, Cyclophosphamide, Dexamethason); VMP (Bortezomib, Melphalan, Prednisone); VRD (Bortezomib, lenalidomide, dexamethasone); R-CHOP (Rituximab, Cyclophosphamide, Adriamycin, Vincristin, Prednisone); Ara-C (Cytarabine), TAD (Thalidomide, Adriamycin, Dexamethasone); CTD (Carfilzomib, Thalidomide, Dexamethasone); BEAM (Carmustine, Etoposide, Ara-C (Cytarabine), Melphalan). Figure 1-figure supplement 1 shows the absolute leukocytes, neutrophils, lymphocytes and monocytes numbers over time after autoHSCT.

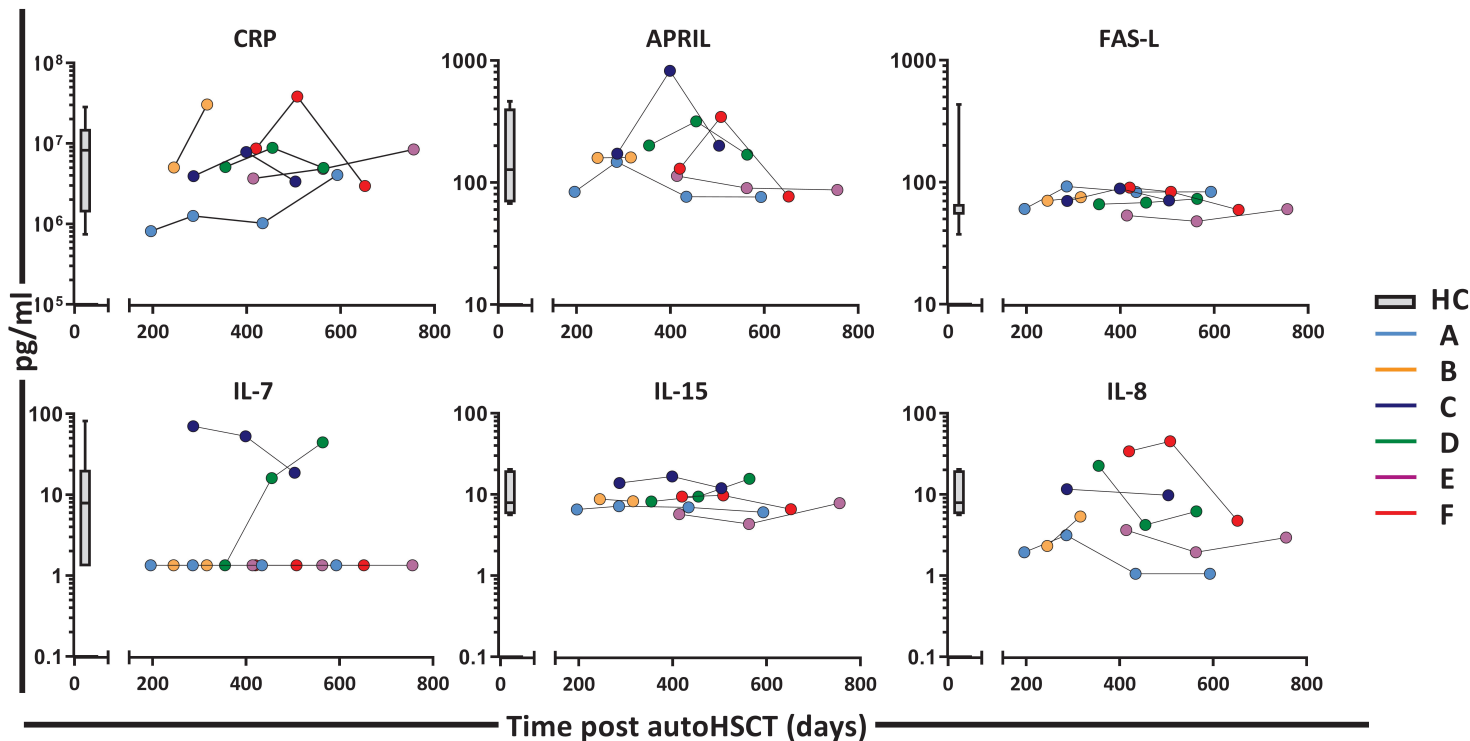


Figure 2. Plasma levels of CRP, APRIL, FAS-L, IL-7, IL-15 and IL-8 post-autoHSCT. Plasma concentration (picogram per milliliter) of CRP (C-reactive protein), APRIL (A proliferation-inducing ligand), FAS-L (FAS ligand), IL-7 (Interleukin 7), IL-15 (Interleukin 15) and IL-8 (Interleukin 8) in patients A to F at different time points after autoHSCT. Box plots represent the distribution of values for healthy controls (n=29, box=25th -75th percentile, black line=median, whiskers=min and max values and Figure 2-Source data 1: Luminex individual values plasma markers) IL-7 levels which were below the level of detection (1.3 pg/ml) were set at 1.

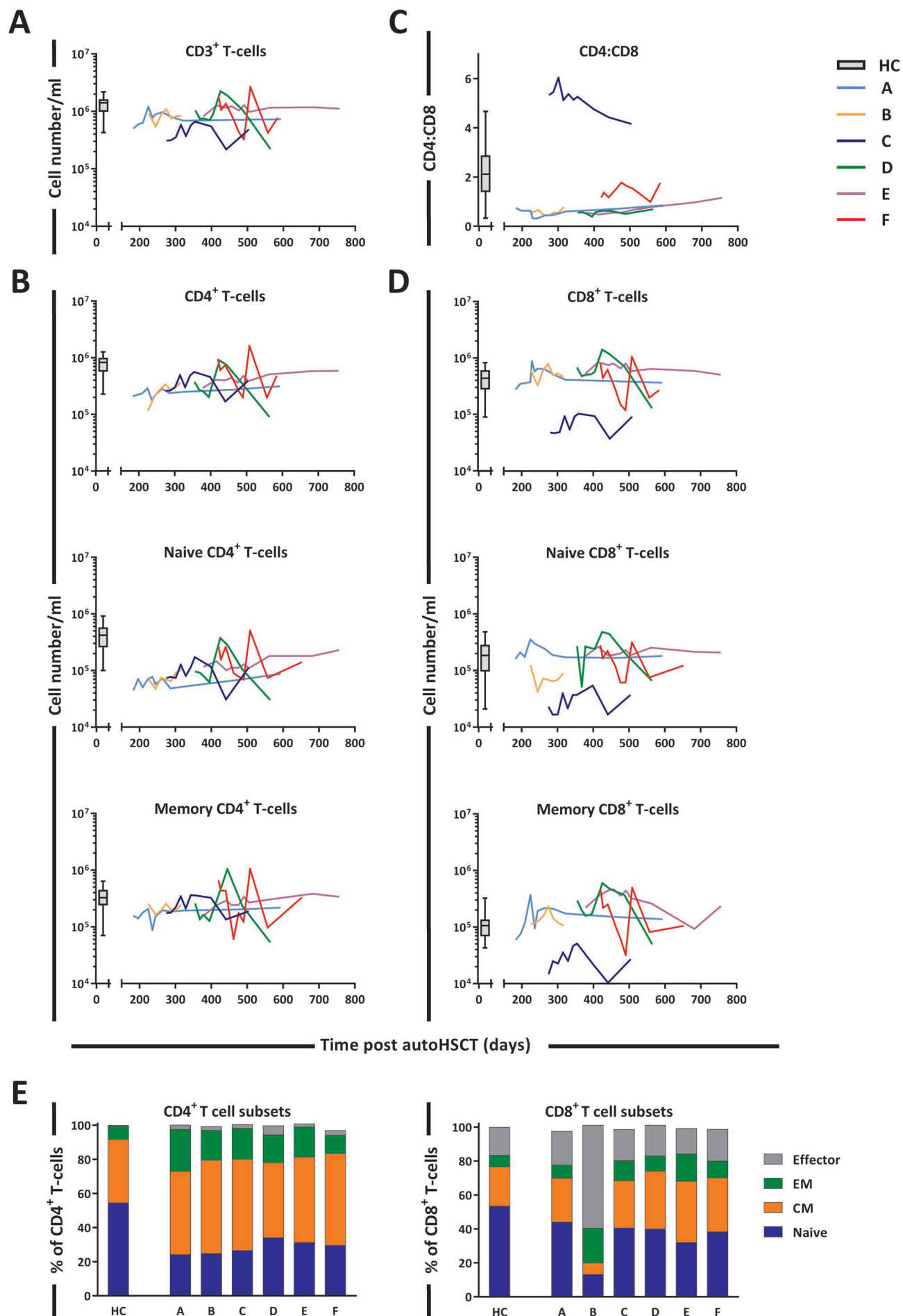
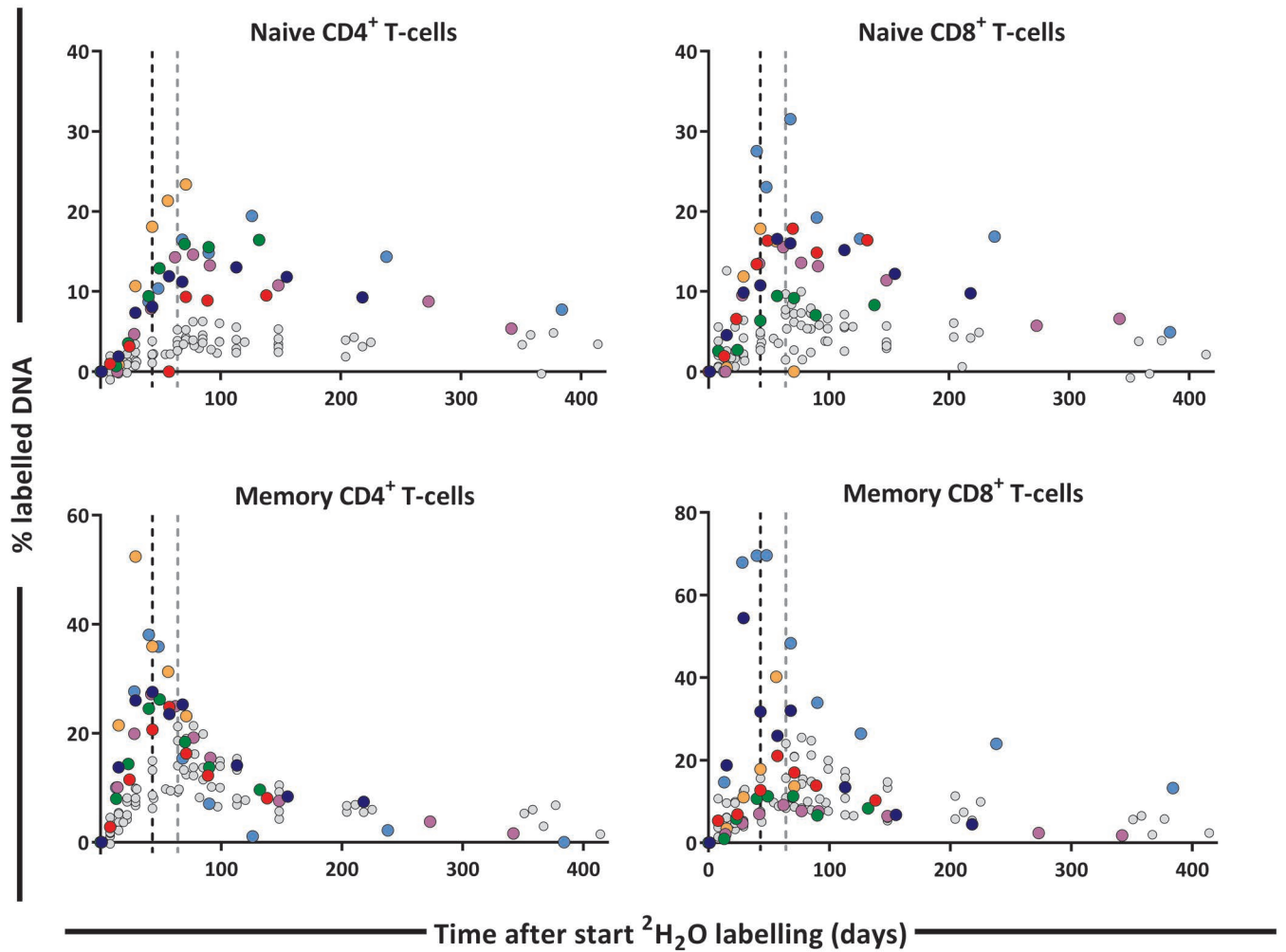


Figure 3. T-cell reconstitution following autoHSCt. Absolute numbers (cells per milliliter) of (A) total CD3⁺ T-cells, (B) total, naive (CD27⁺CD45RO⁻) and memory (CD45RO⁺) CD3⁺CD4⁺ T-cells, (D) total, naive (CD27⁺CD45RO⁻) and memory (CD45RO⁺) CD3⁺CD8⁺ T-cells and (C) the CD4:CD8 ratio over time for the duration of the study are depicted. Box plots represent the distribution of values for healthy controls (N=17 for CD3⁺, CD4⁺, CD8⁺ and CD4:CD8 ratio, other N=27, box=25th-75th percentile, black line=median, whiskers=min and max values). Absolute numbers shown in the graph are not normalized. (E) Bar graphs show the median percentage of naive (CD27⁺CD45RO⁻), central memory (CM, CD27⁻CD45RO⁺), effector memory (EM, CD27⁺CD45RO⁺) and effector (CD27⁻CD45RO⁻) CD4⁺ and CD8⁺ T-cells of autoHSCt patients (A to F) and HCs (n=6) in the indicated colors. For the T-cell subset distribution per patient over time see Figure 3-figure supplement 1 and Figure 3-source data 1. For the gating strategy see Figure 3-figure supplement 2.

A



B

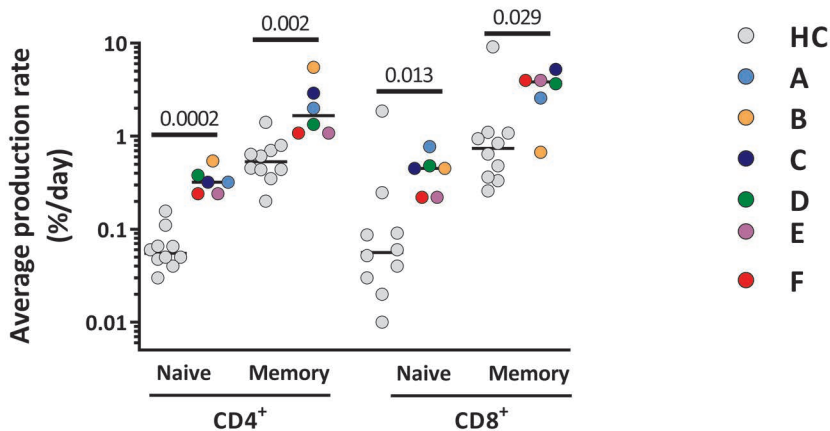


Figure 4. T-cell dynamics after autoHSC. (A) Deuterium enrichment in the DNA of naive and memory CD4^+ and CD8^+ T-cells in autoHSC patients (A to F, color symbols), and healthy controls (HCs, grey symbols)²⁴. Dotted lines correspond to the end of the labelling period (black for autoHSC patients and grey for HCs). Label enrichment was scaled between 0 and 100% by normalizing for the maximum enrichment in granulocytes (Figure 4-figure supplement 1 and Figure 4-source data 1, Parameter estimates urine and granulocytes). (B) Estimates of the per cell production rate of naive and memory CD4^+ and CD8^+ T-cells in autoHSC patients and HCs²⁴ (for individual fits and parameters estimates see Figure 4-figure supplement 2 and Figure 4- source data 2). Different symbols indicate different individuals, autoHSC patients (A to F) in color and HCs in grey. Horizontal lines represent median values. P-values between groups are shown (Mann-Whitney test). For total daily production see Figure 4-figure supplement 3. For information on modeling in R see Figure 4-source code1.

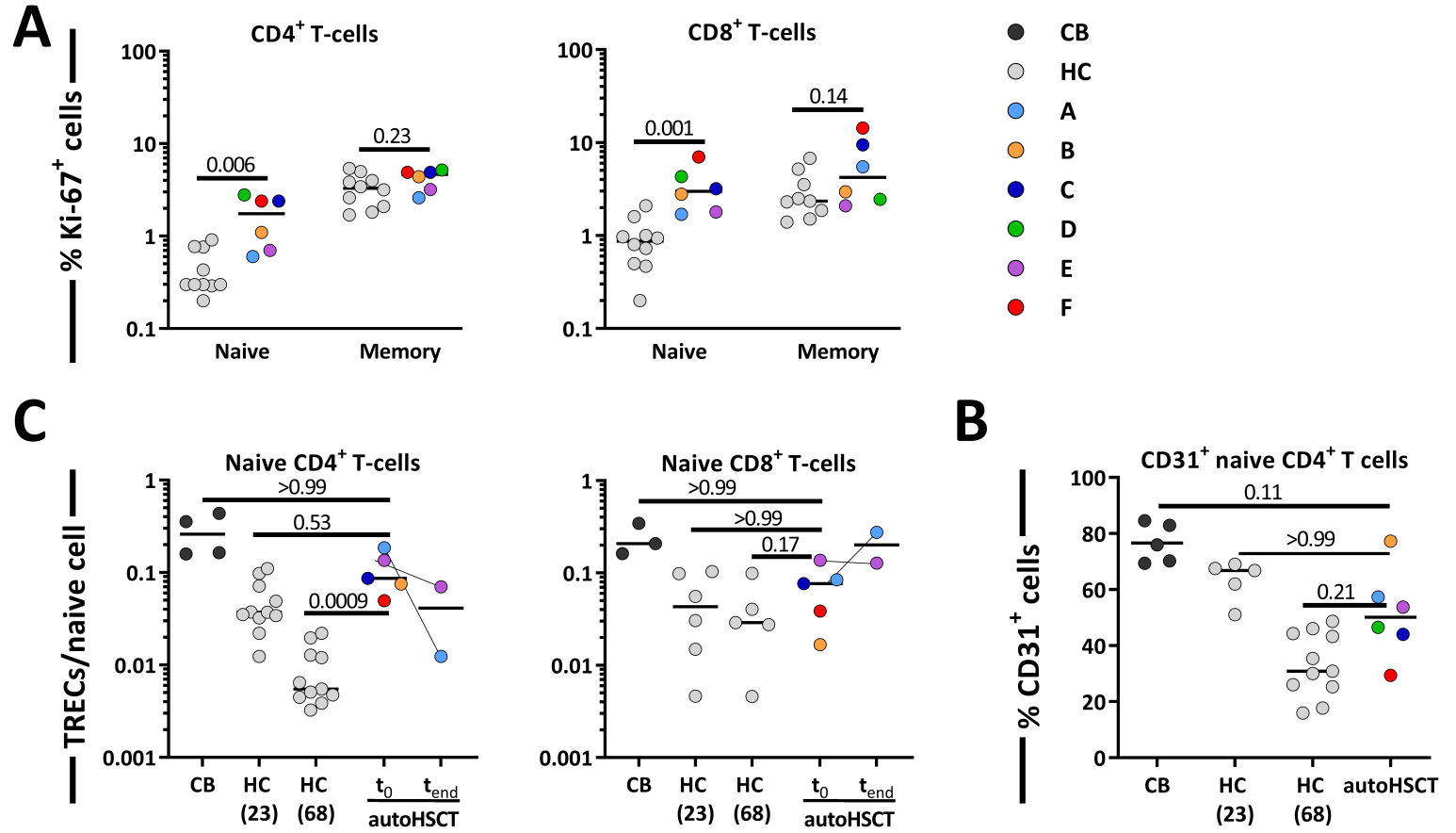


Figure 5. Contribution of peripheral proliferation and thymic output to T-cell production after autoHSCT. (A) Ki-67 expression was measured within naive and memory CD4⁺ (left panel) and CD8⁺ (right panel) T-cell in autoHSCT patients and HCs²⁴ (for gating strategy see Figure 5-figure supplement 1). (B) Average number of TRECs per naive CD4⁺ (left panel) and CD8⁺ (right panel) T-cell in autoHSCT patients, cord blood (CB) and HCs²⁴. For Patient A and Patient E, TREC content was measured the first day of the study (t_0) as well as the last study visit (t_{end}). For Patient D, TREC content was not successfully measured due to limited material. (C) CD31 expression was measured within naive CD4⁺ T-cells in autoHSCT patients, cord blood and HCs²⁴. For changes in CD31 expression and absolute numbers of CD31⁺ cells over time, see Figure 5-figure supplement 2. Different symbols indicate different individuals, autoHSCT patients (A to F) in color, CB in dark grey, and young (median age of 23 years) and old (median age of 68 years) HCs in light grey. Horizontal lines represent median values. P-values of differences between groups are shown (Mann-Whitney test (A) and Kruskal-Wallis with Dunn's correction (B), comparison with CB, HC (23) and HC (68)).

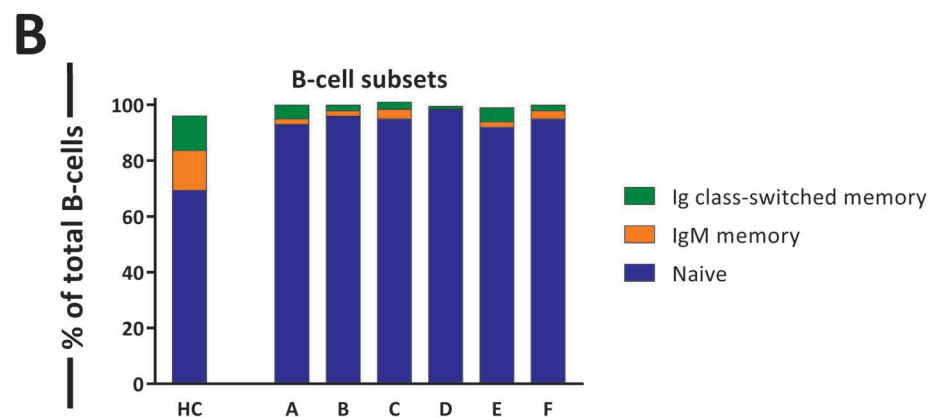
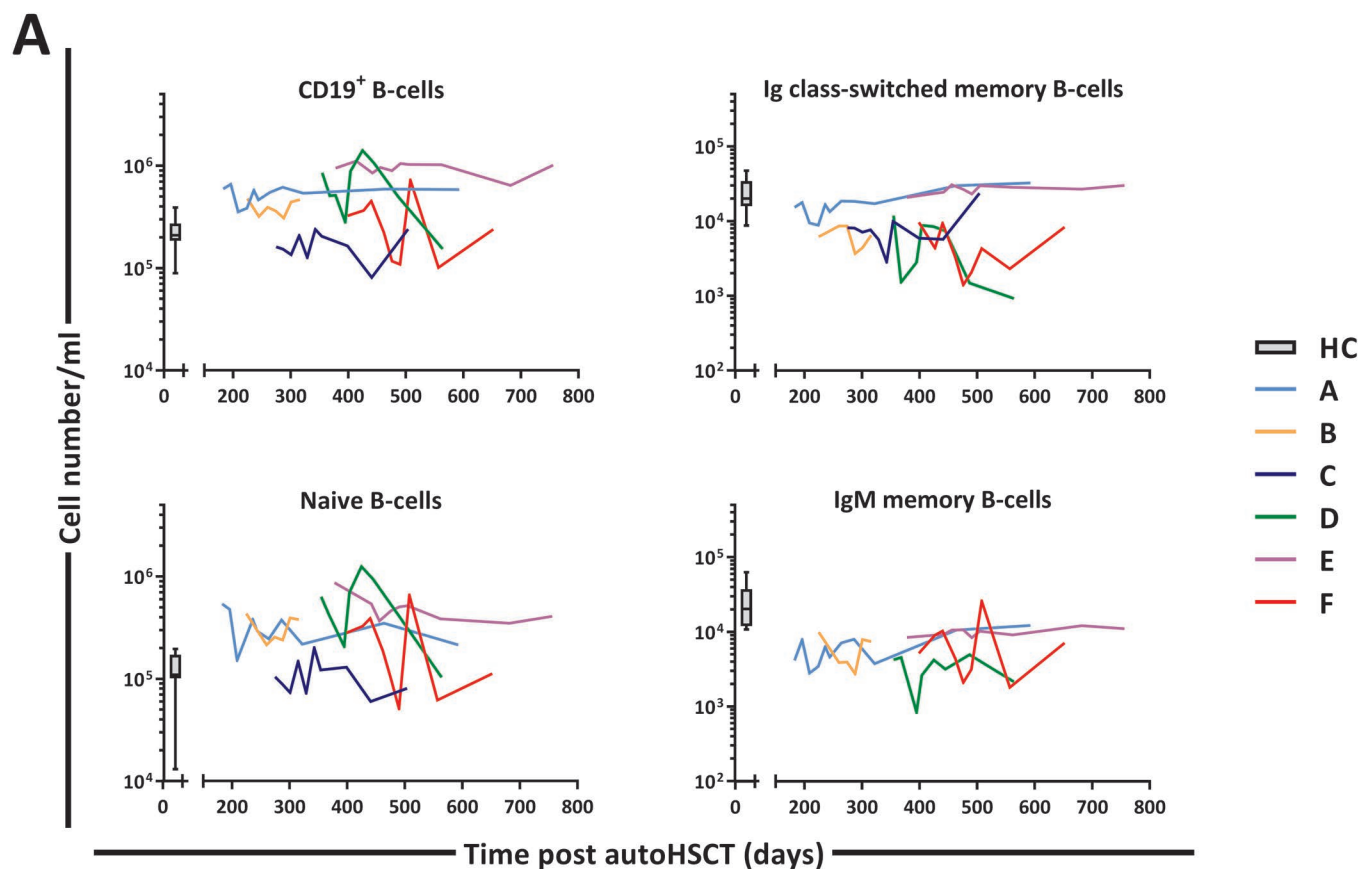


Figure 6. B-cell reconstitution following autoHSCT. (A) Absolute numbers (cells per milliliter) of total CD19⁺ B-cells, naive (CD19⁺IgM⁺CD27⁻), Ig class-switched memory (CD19⁺IgM⁻CD27⁺) and IgM⁺ memory (CD19⁺IgM⁺CD27⁺) B-cells in peripheral blood over time. Graphs show the absolute cell counts per milliliter in autoHSCT patients (patients A to F) over the duration of the study. Box plots represent the distribution of values for healthy controls (N=10, box=25th-75th percentile, black line=median, whiskers=min and max values). Absolute numbers shown in the graph are not normalized. (B) Bar graphs show the median percentage of naive, Ig class-switched memory and IgM⁺ memory B-cells within total CD19⁺ B-cells of autoHSCT patients (patients A to F) and HCs (N=10). For the B-cell subset distribution per patient over time see Figure 6-figure supplement 1 and Figure 6-source data 1). Note the different y-axes in panel A.

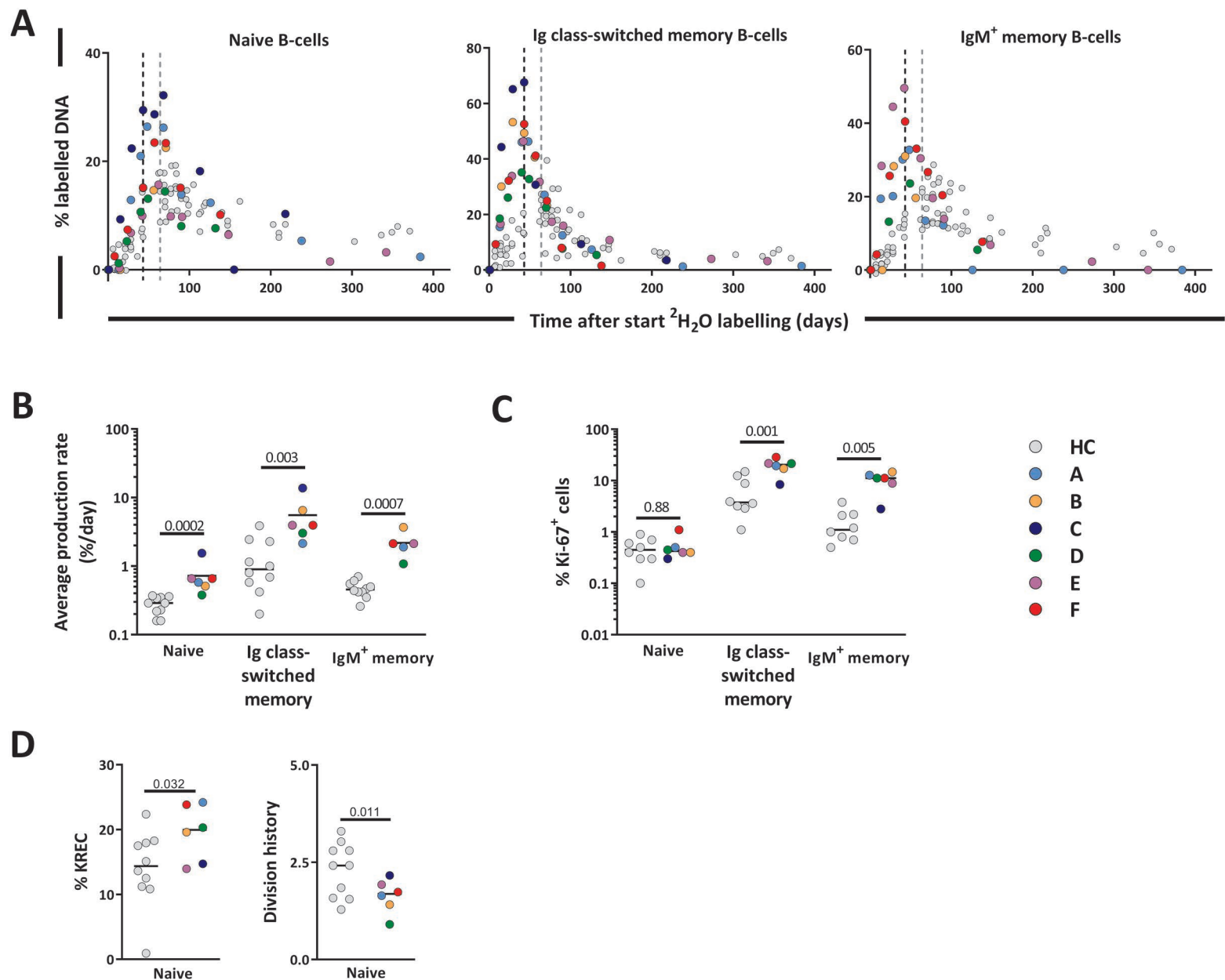


Figure 7. B-cell dynamics after autoHSCT. (A) Deuterium enrichment in the DNA of B cell subsets in autoHSCT patients (A to F, color symbols), and HCs (grey symbols)²⁴. Dotted lines correspond to the end of the labelling period (black for autoHSCT patients and grey for HCs). Label enrichment was scaled between 0 and 100% by normalizing for the maximum enrichment in granulocytes (Figure 4-source data 1: Parameter estimates urine and granulocytes). **(B)** Estimates of the per cell production rates of naive, Ig class-switched memory and IgM⁺ memory B-cells in autoHSCT patients and HCs²⁴. For individual fits and estimates see Figure 7-figure supplement 1 and Figure 7-source data 1 **(C)** Ki-67 expression was measured within naive, Ig class-switched memory and IgM⁺ memory B-cells in autoHSCT patients and HCs²⁴ (for gating strategy see Figure 5-figure supplement 1). **(D)** Percentage of naive B-cells containing a KREC and naive B-cell division history for autoHSCT patients and HCs²⁴. Different symbols indicate different individuals, autoHSCT patients (A to F) in color and HCs in grey. Horizontal lines represent median values. P-values of differences between groups are shown (Mann-Whitney test). For information on modeling in R see Figure 4-source code 1.

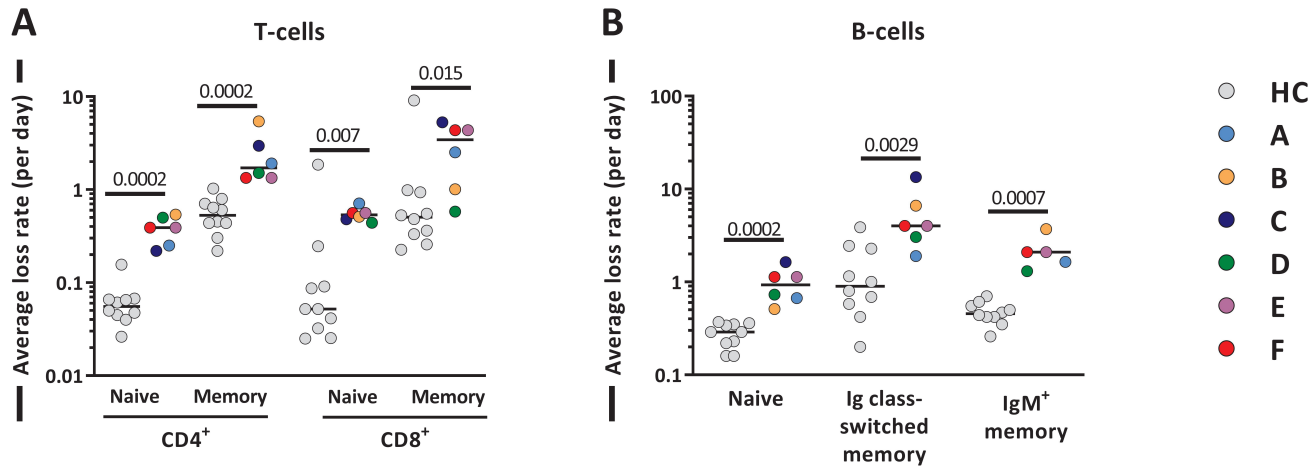


Figure 8. Average T-cell and B-cell loss rates following autoHSCT. (A) Estimates of the average loss rates of naive and memory CD4⁺ and CD8⁺ T-cells and of (B) naive, Ig class-switched memory and IgM⁺ memory B-cells in autoHSCT patients (A to F, color symbols), and HC (grey symbols)²⁴. Average loss rates were calculated (see Figure 8-source data 1) using the estimated average production rates and the corrected cell numbers (Figure 8-figure supplement 1 and 2) as described in material and methods. Horizontal lines represent median values. P-values of differences between groups are shown (Mann-Whitney test).

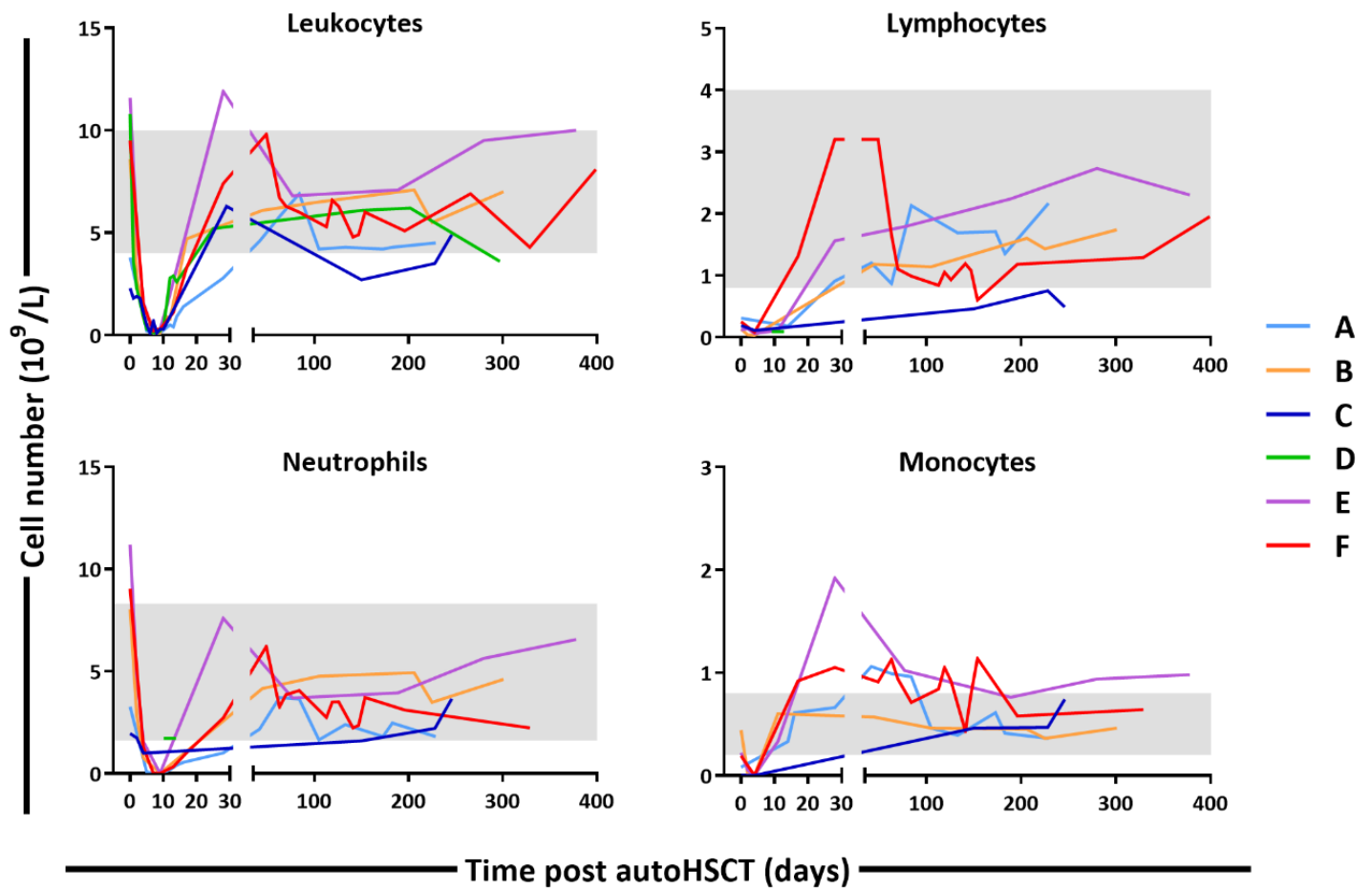


Figure 1-figure supplement 1. Absolute numbers (cells $\times 10^9$ per liter of blood) of leukocytes, neutrophils, lymphocytes and monocytes in peripheral blood of autoHSCT patients (patients A to F) over time after autoHSCT obtained by automated blood leukocyte differential count (leukodiff). Grey areas show the range of healthy individuals' values

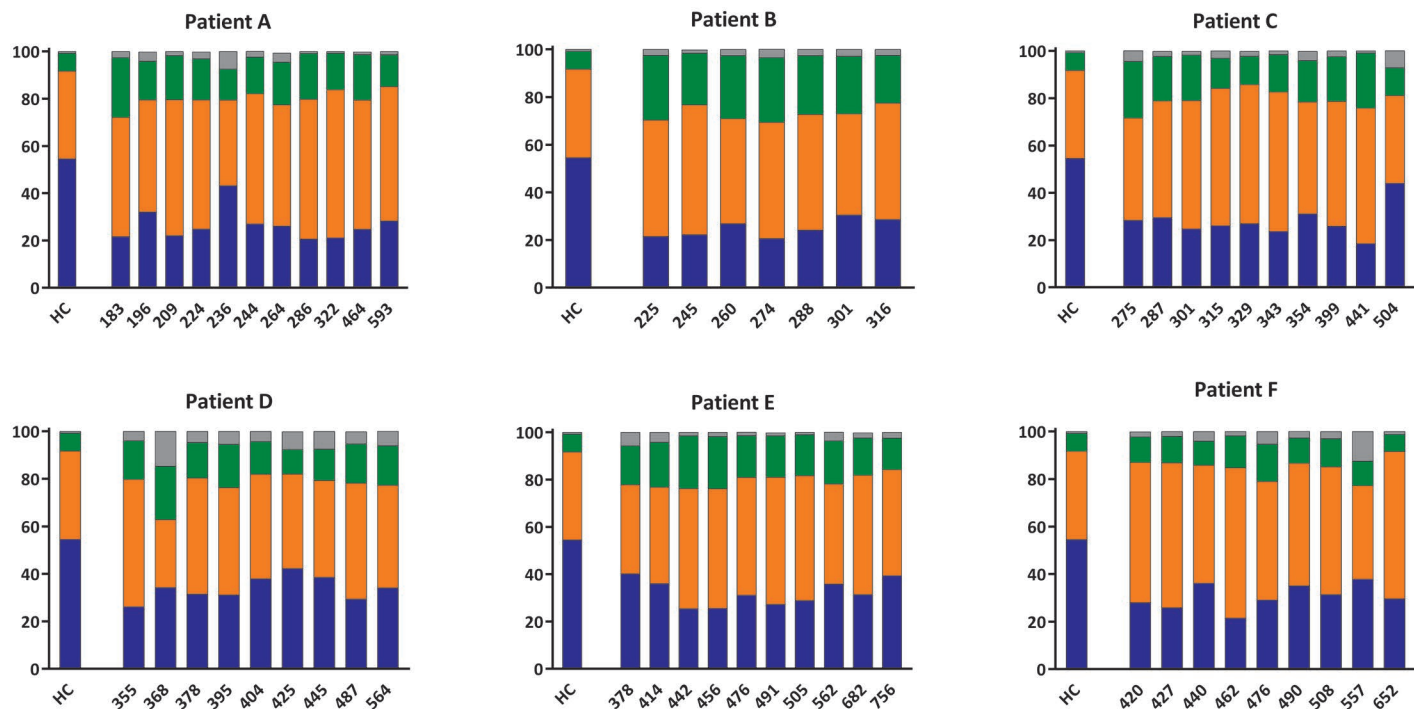
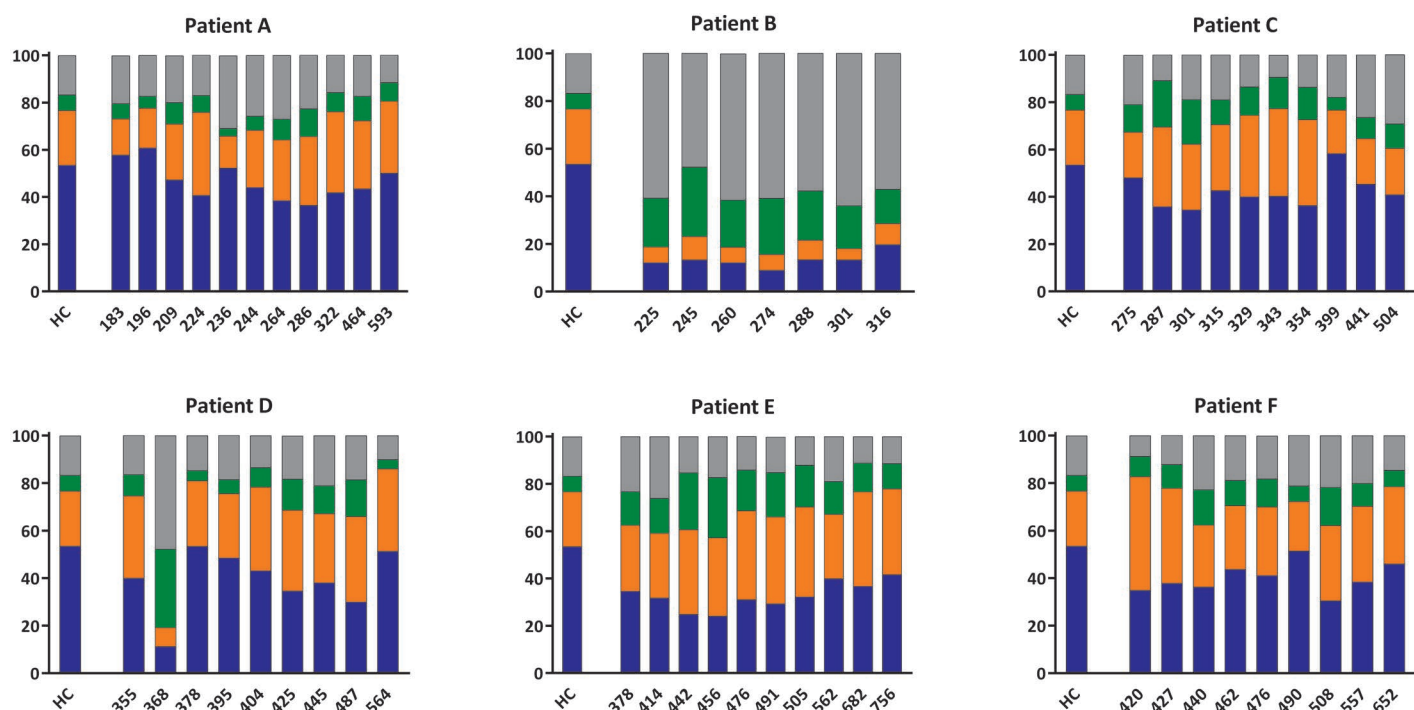
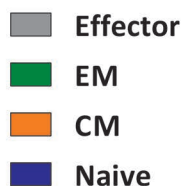
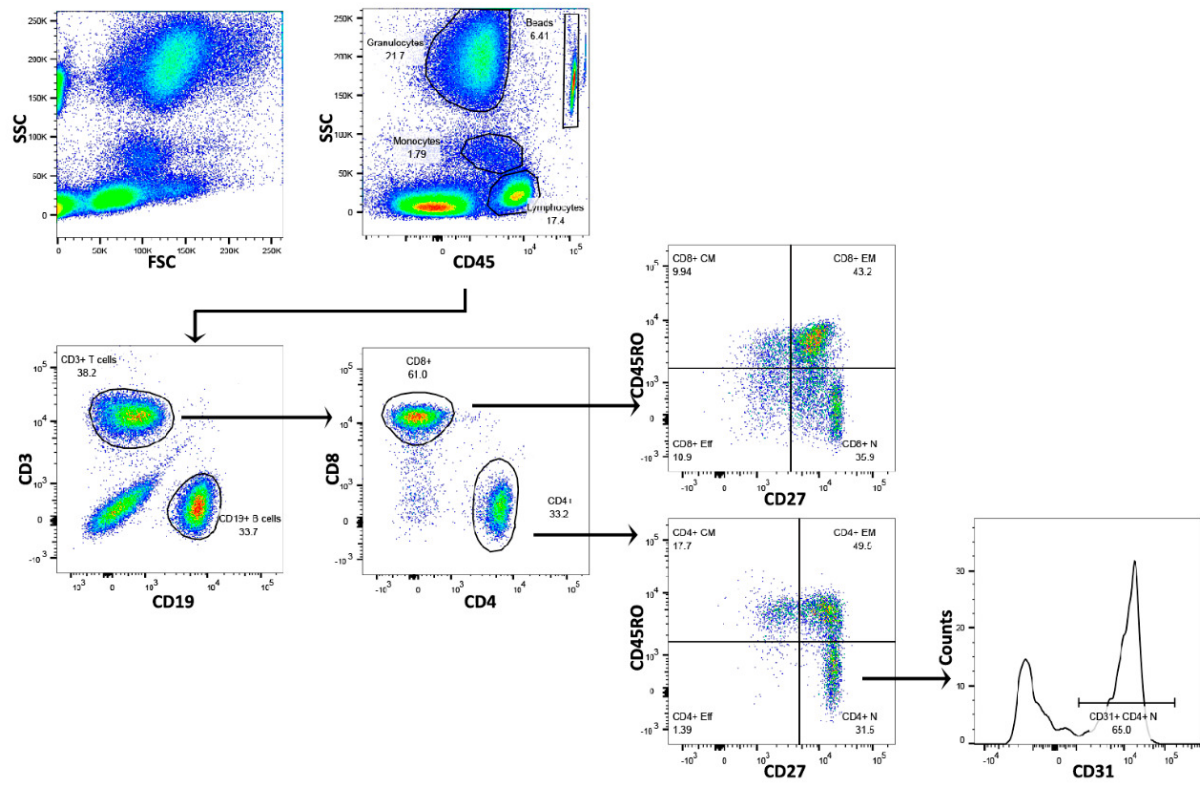
A**% of CD4⁺ T-cells****B****% of CD8⁺ T-cells****Time post autoHCT (days)**

Figure 3-figure supplement 1. T-cell subset distribution per autoHCT patient over time. Percentage of naive T-cells (blue), central memory T-cells (CM, orange), effector memory T-cells (EM, green) and effector T-cells (effector grey) within (A) CD4⁺ or (B) CD8⁺ T-cells at the study times after autoHCT (patients A to F). Bar graphs for HCs (N= 6) show the median percentage of naive, CM, EM and effector T-cells within CD4⁺ or CD8⁺ T-cells.

A TruCount



B Sorting strategy

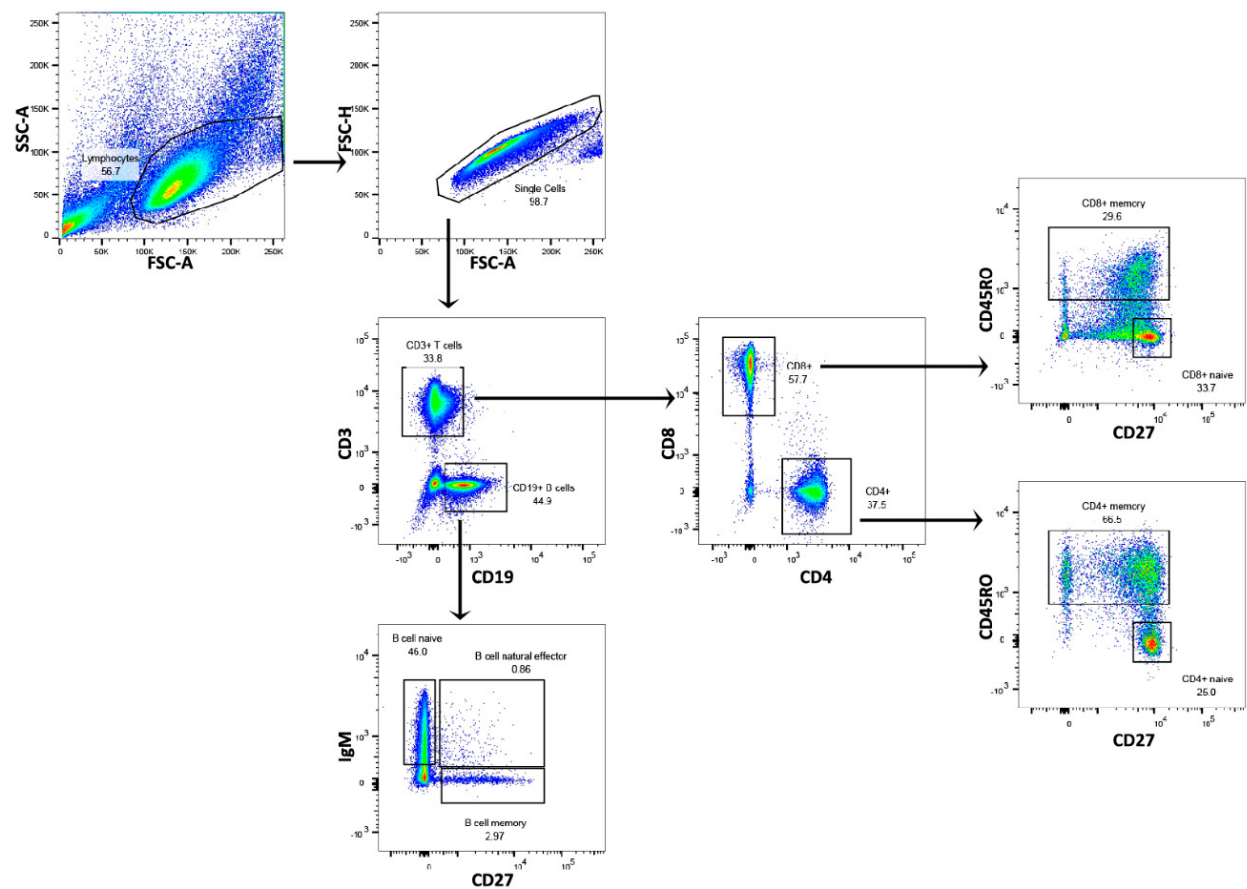


Figure 3-figure supplement 2. Gating strategy for TruCount and cell sorting. (A) TruCount gating strategy for naive ($CD27^+CD45RO^-$), central memory (CM, $CD27^+CD45RO^+$), effector memory (EM, $CD27^+CD45RO^+$) and effector ($CD27^-CD45RO^-$) $CD4^+$ and $CD8^+$ T-cells and B-cells. **(B)** Gating strategy for sorting for naive ($CD27^+CD45RO^-$) and memory ($CD45RO^+$) $CD4^+$ and $CD8^+$ T-cells and for naive (IgM^+CD27^-), Ig class-switched memory (IgM^-CD27^+) and IgM^+ memory (IgM^+CD27^+) B-cells.

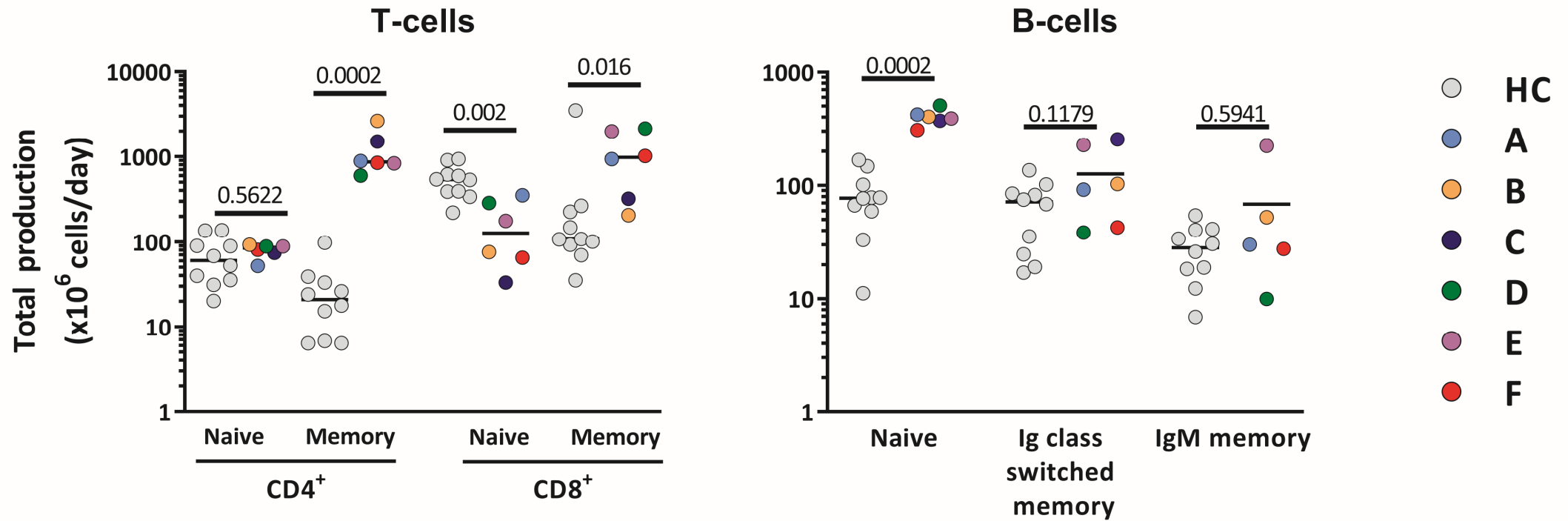
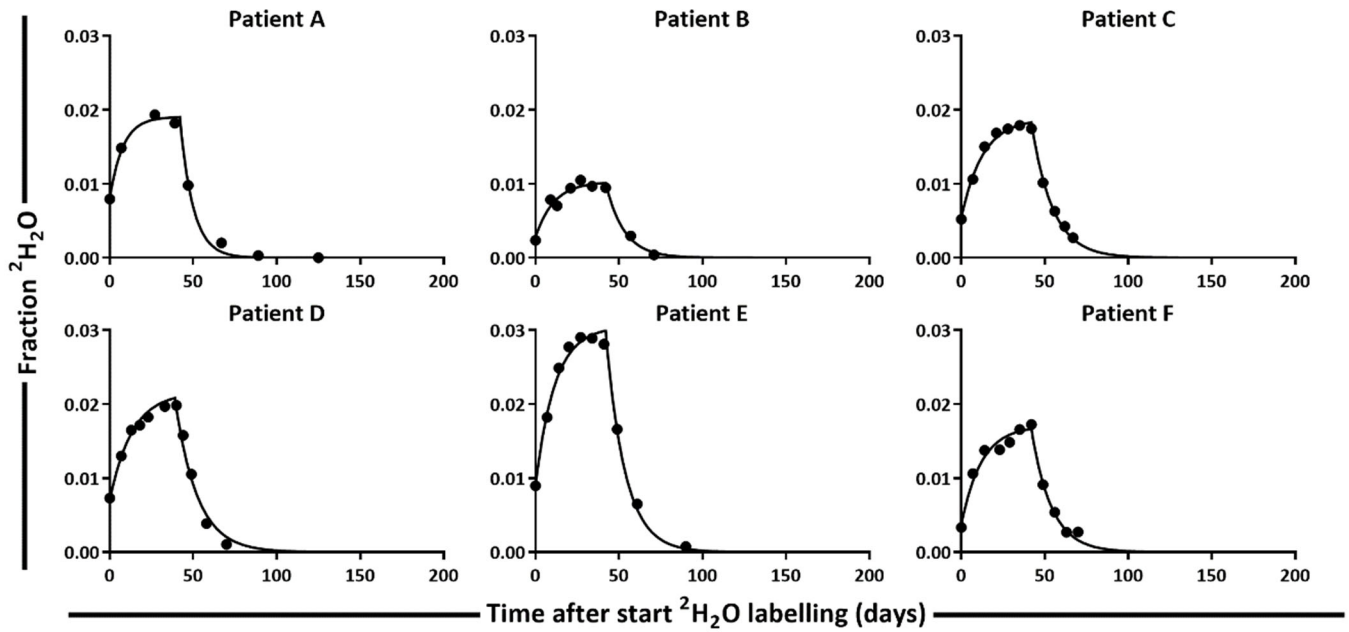


Figure 4-figure supplement 3. Total daily production T-cell and B-cell subsets, calculated as $(\sigma/N + p_{-}(N)) \times (\text{absolute number of cells per liter of blood}) \times (5 \text{ liter blood}) \times 50$, assuming that 2% of lymphocytes reside in the blood³⁴. Horizontal lines represent median values. P-values of differences between groups are shown (Mann-Whitney test).

A Body water



B Granulocytes

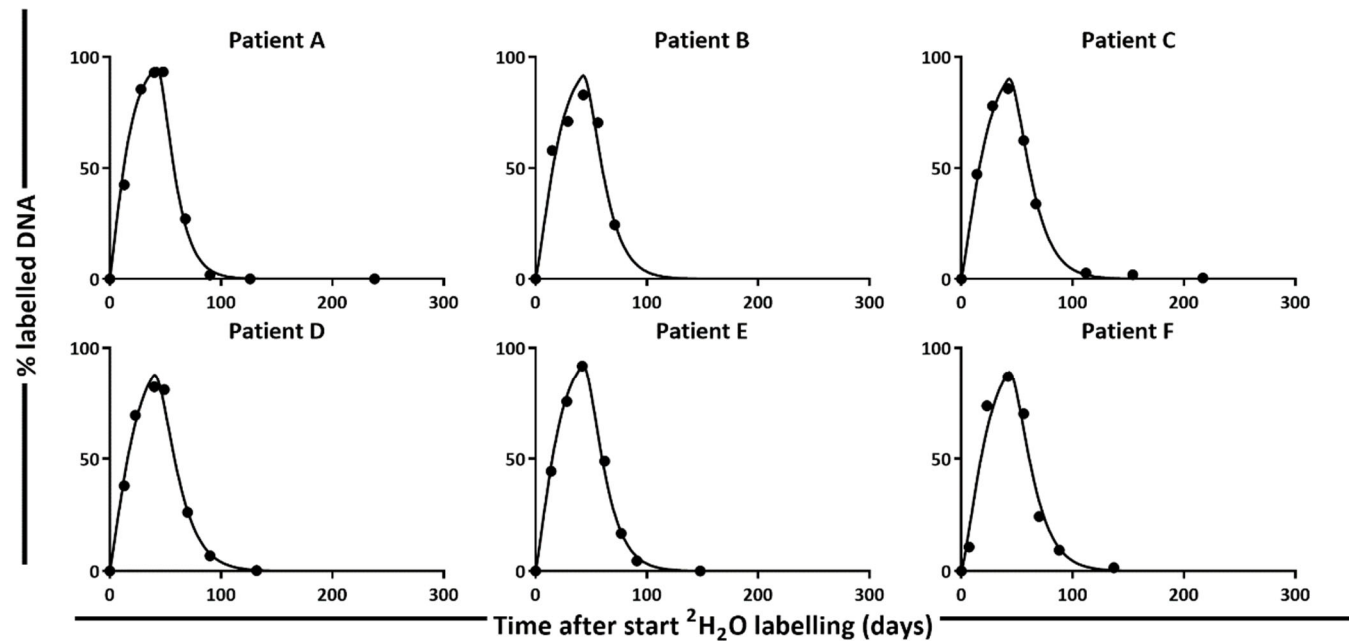


Figure4-figure supplement 1. Best fits of ^2H enrichment in (A) body water (urine) and (B) granulocytes from the 6 autoHSCT patients (A to F). The estimated parameters for urine and granulocytes can be found in Figure 4-source data 2: Parameter estimates urine and granulocytes.

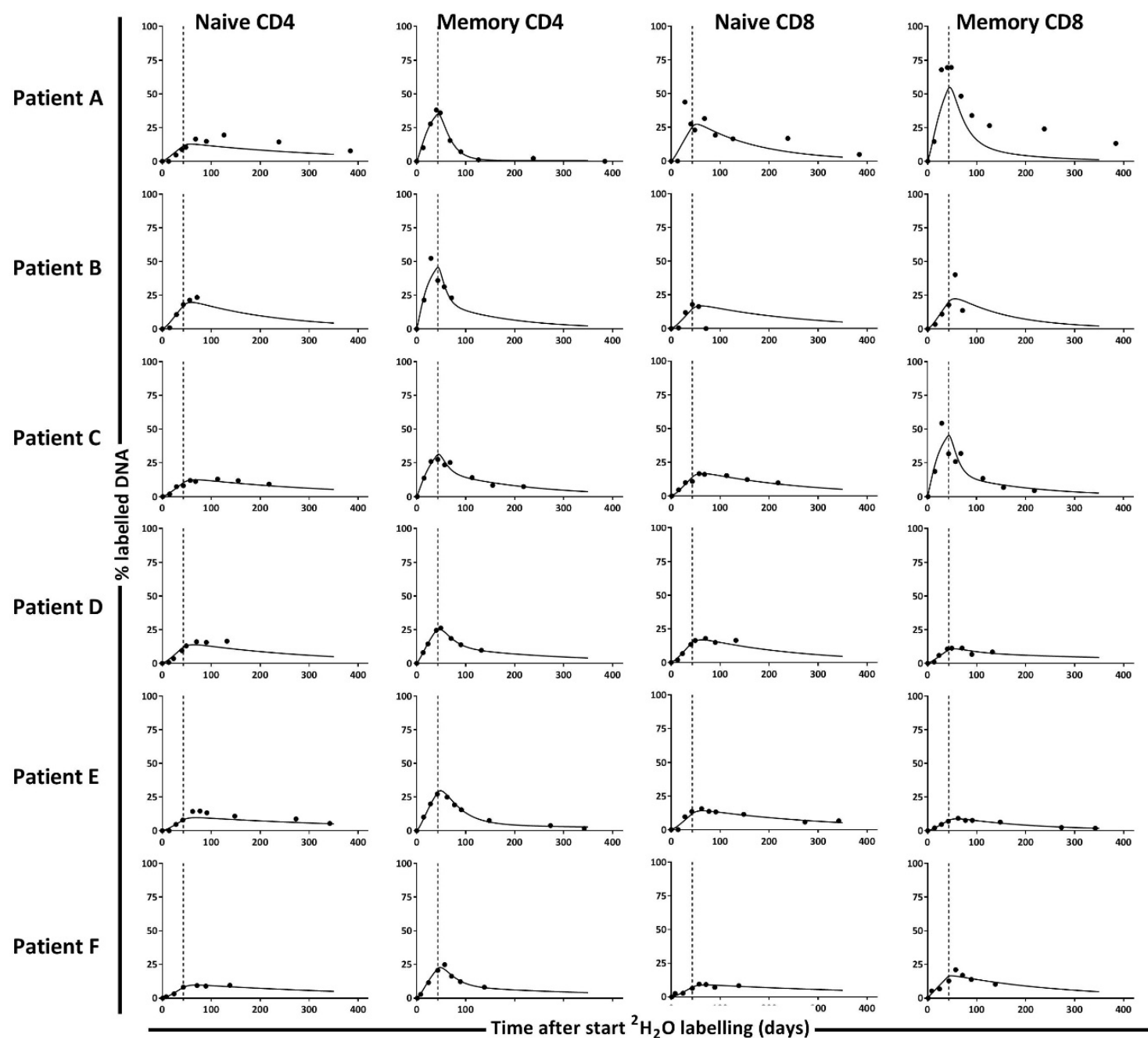
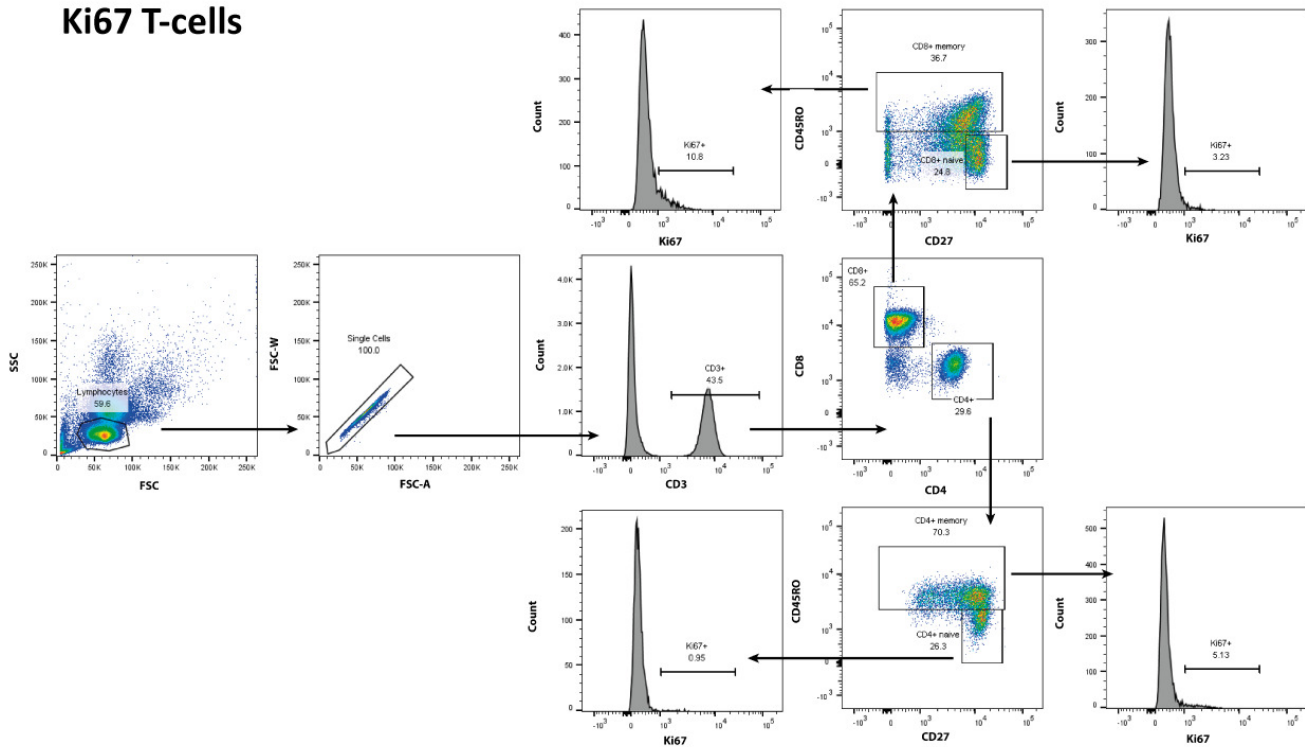


Figure 4-figure supplement 2. Best fits of ^2H enrichment in T-cell subsets in autoHSCT patients. Best fits of the model (see material and methods) to the enrichment data in naive and memory CD4^+ and CD8^+ T cells in the 6 autoHSCT patients (A to F). Measured enrichments are shown by black dots. Label enrichment in the DNA was scaled between 0 and 100% by normalizing for the maximum enrichment in granulocytes (see material and methods). The end of $^2\text{H}_2\text{O}$ administration is marked by a dashed vertical line. Best fits of ^2H enrichment of the corresponding subsets in healthy individuals were previously published by Westera *et al.* 2015²⁴.

Ki67 T-cells



Ki67 B-cells

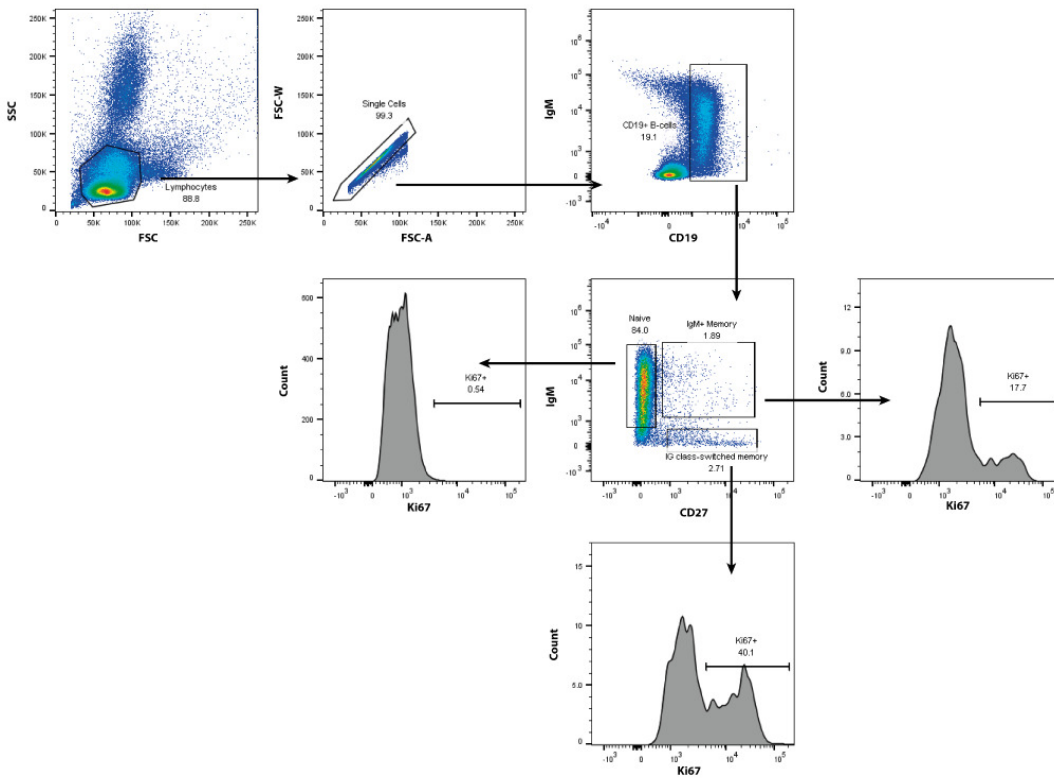


Figure 5-figure supplement 1. Gating strategy for Ki-67 expression of T and B cell subsets. Gating strategy for Ki-67 expression of naive ($CD27^+CD45RO^-$) and memory ($CD45RO^+$) $CD4^+$ and $CD8^+$ T-cells and naive (IgM^+CD27^-), Ig class-switched memory (IgM^+CD27^+) and IgM^+ memory (IgM^+CD27^+) B-cells

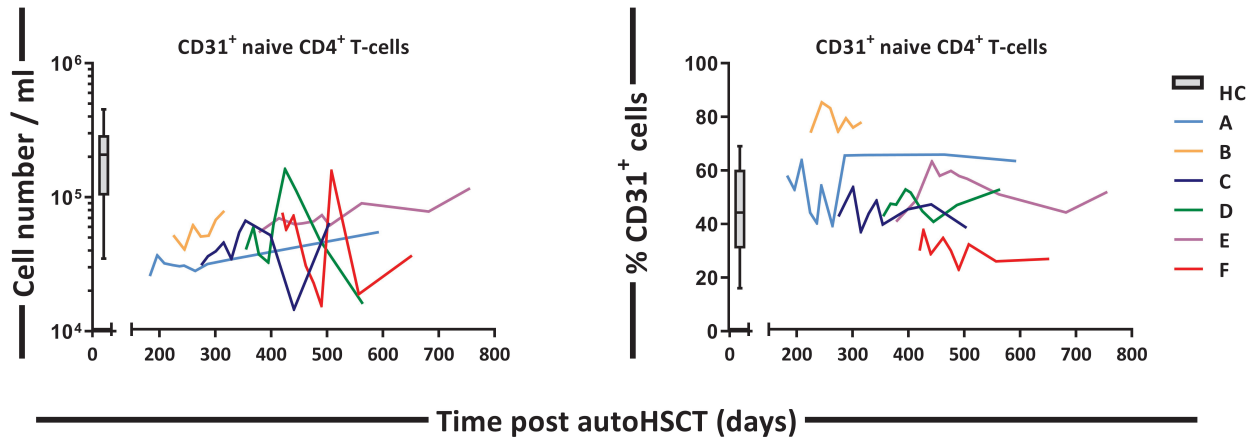
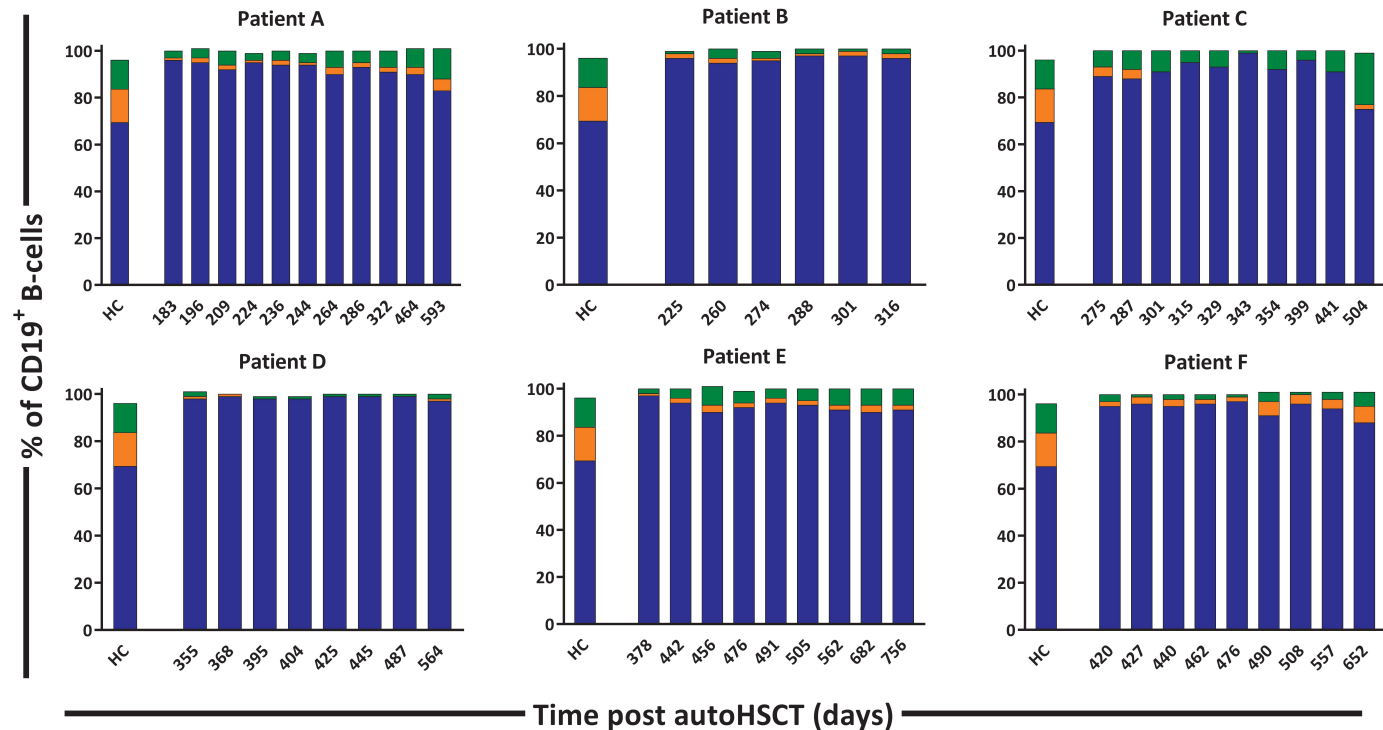


Figure 5-figure supplement 2. CD31 expression in naive CD4⁺ T-cells over time. Absolute numbers of CD31⁺ naive CD4⁺ T-cells per milliliter of blood over time (left panel) and percentage CD31⁺ cells within naive CD4⁺ T-cells (right panel). Graphs show the absolute cell counts per milliliter or the percentage CD31⁺ cells in autoH SCT patients (patients A to F, in color) over time for the duration of the study. Box plots represent the distribution of values for healthy controls (N=23, box=25th-75th percentile, black line=median, whiskers=min and max values). Absolute numbers shown in the graph are not normalized.



■ Ig switched memory
■ IgM memory
■ Naive

Figure 6-figure supplement 1 . B-cell subset distribution per autoHSCT patient over time. Percentage of naive B-cells (blue), IgM⁺ memory B-cells (orange) and Ig class-switched memory B-cells (green) within total CD19⁺ B-cells per patient (patients A-F) at the study times after autoHSCT. Bar graphs for HCs show the median percentage of naive, memory and natural effector B-cells within total CD19⁺ B-cells. For the gating strategy see Figure 3-figure supplement 1.

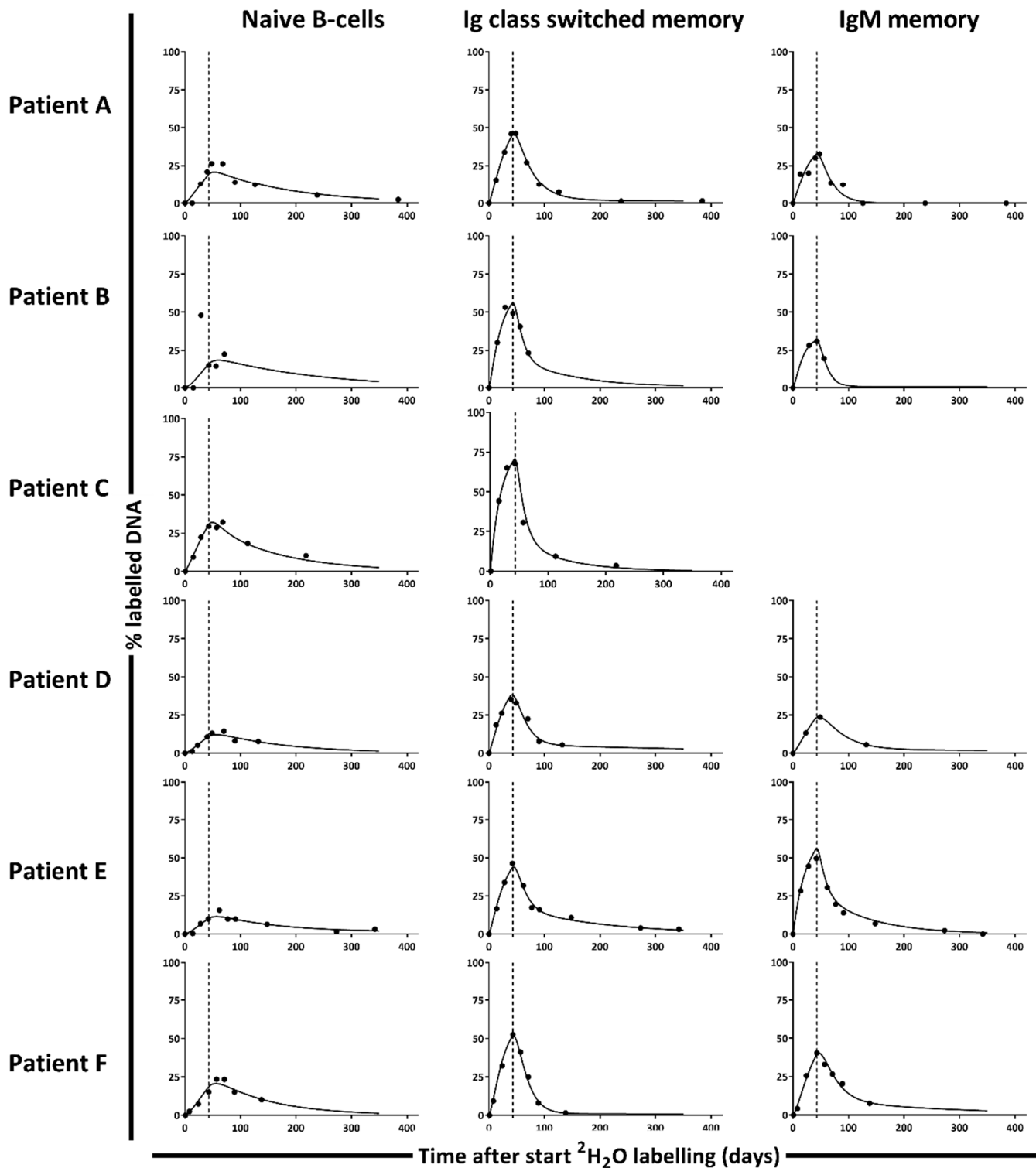


Figure 7-figure supplement 1. Best fits of ^2H enrichment in B-cell subsets in autoHSCT patients. Best fits of the model (see material and methods) to the enrichment data in naive, Ig class-switched memory and IgM⁺ memory B-cells in the 6 autoHSCT patients (A to F). Measured enrichments are shown by black dots. Label enrichment in the DNA was scaled between 0 and 100% by normalizing for the maximum enrichment in granulocytes (see material and methods). The end of $^2\text{H}_2\text{O}$ administration is marked by a dashed vertical line. Best fits of ^2H enrichment of the corresponding subsets in healthy individuals were previously published by Westera *et al.* 2015 ²⁴.

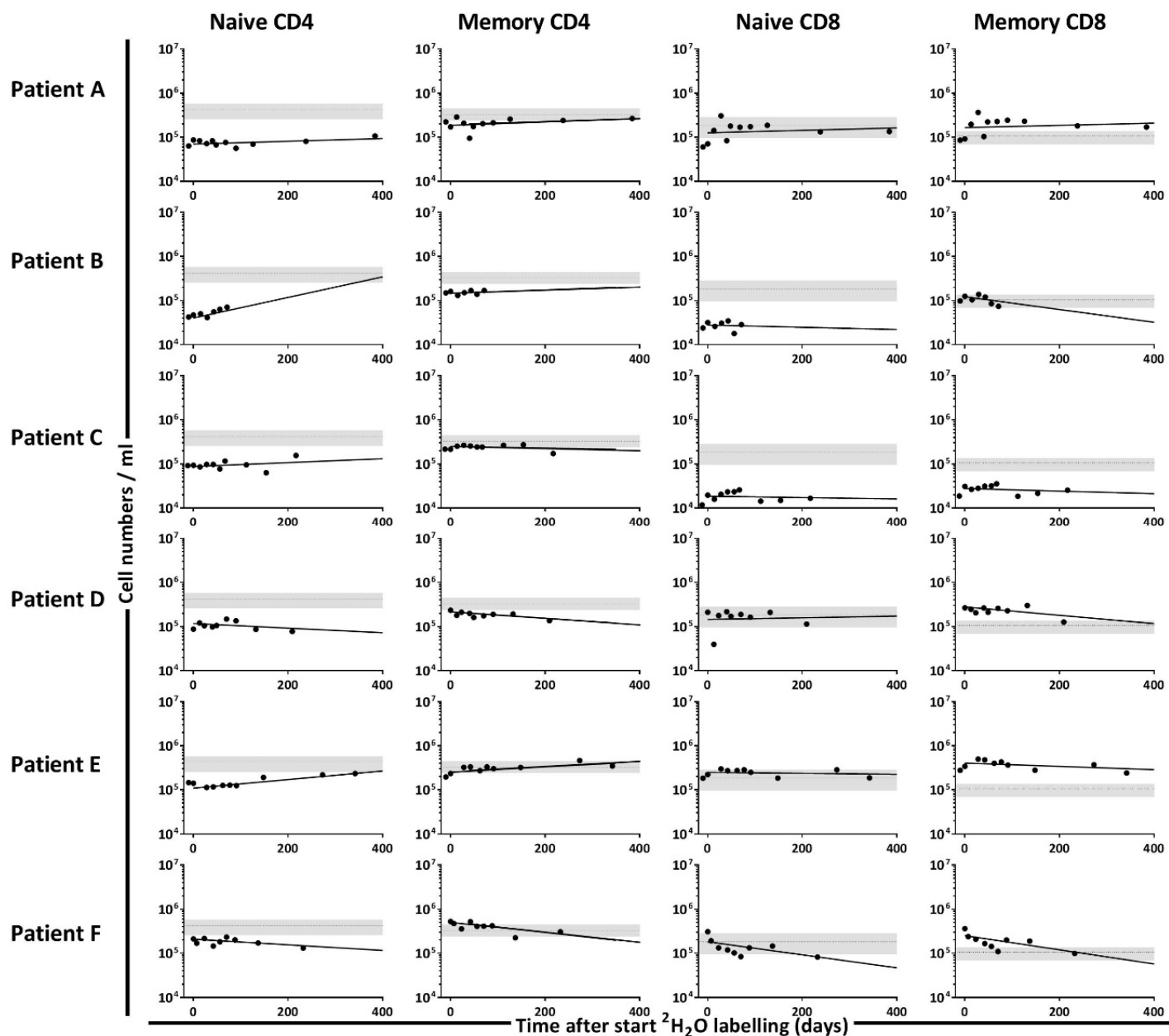


Figure 8-figure supplement 1. Best fits of T-cell numbers in autoHSCT patients. Best fits (black lines) to the normalized cell numbers data (black dots). Absolute numbers (cells per milliliter of blood) of naive ($CD27^+CD45RO^-$) and memory ($CD45RO^+$) $CD4^+$ and $CD8^+$ T-cells were corrected for noise as described in material and methods. The median cell numbers (dotted grey line) and the corresponding IQR (interquartile range, grey area) for healthy controls are shown.

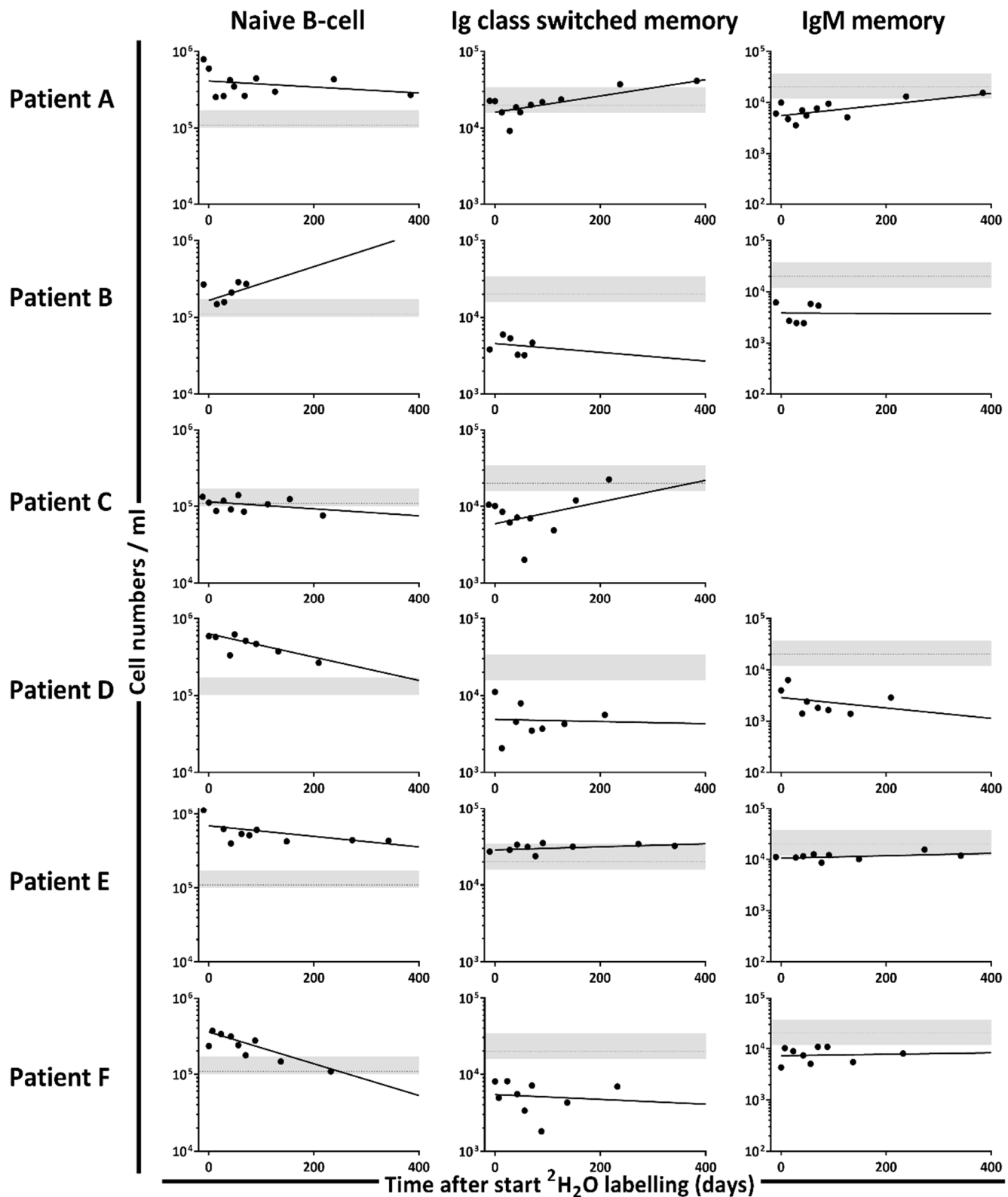


Figure 8-figure supplement 2. Best fits of B-cell numbers in autoHSCt patients. Best fits (black lines) to the normalized cell number data (black dots). Absolute numbers (cells per milliliter of blood) of naive ($\text{CD}19^+\text{IgM}^+\text{CD}27^-$), Ig class-switched memory ($\text{CD}19^+\text{IgM}^-\text{CD}27^+$) and IgM⁺ memory ($\text{CD}19^+\text{IgM}^+\text{CD}27^+$) B-cells were corrected for noise as described material and methods. The median cell numbers (dotted grey line) and the corresponding IQR (interquartile range, grey area) for healthy controls are shown.